NASA TECHNICAL MEMORANDUM

NASA TM X–62,051

NASA TM X–62,051

WINDWARD SURFACE HEATING ON THE MSC ORBITER FUSELAGE

George G. Mateer

Ames Research Center
Moffett Field, Calif. 94035

August 1971

WINDWARD SURFACE HEATING ON THE MSC ORBITER FUSELAGE

By

George G. Mateer

SUMMARY

Heat-transfer data were obtained on the windward surface of the Manned Spacecraft Center (MSC) orbiter fuselage (without wings) at a freestream Mach number of 7.4 and angles of attack from 40° to 70°. Heating and transition data have been compared with appropriate theories and correlations, and some effects of surface roughness have been simulated. Conclusions of the study are: 1) Laminar heating is predictable by simple, modified-swept-cylinder theory; 2) Initial boundary-layer transition correlations proposed for the shuttle are somewhat conservative for the present data; 3) Surface roughness was sufficient to cause premature transition and local increases of 20% in transitional and turbulent heating rates.

SYMBOLS

c	specific heat
h	wire height
k	thermal conductivity
L	model axial length from nose to trailing edge of horizontal stabilizer
M	Mach number
p	pressure
$\dot{q}$	heat-transfer flux
Re/l	Reynolds number per unit length
Re_θ	Reynolds number based on momentum thickness
T	temperature
u	velocity
x	axial length from nose
x_t	axial length to transition
α	angle of attack
δ	boundary-layer thickness
ρ	density
μ	viscosity

Subscripts

e	boundary-layer-edge condition
s	sphere
t	total condition
∞	freestream condition

INTRODUCTION

The successful design of the space shuttle transportation system is, in part, contingent on providing a broad data base from which to evaluate technology requirements and configuration concepts. Since much of the aerothermodynamic technology is based on emperical theories or correlations, the need for experimental data is particularly important. Consequently, this investigation was one of many undertaken to provide aerodynamic heating data on proposed space shuttle configurations.

In the present study the MSC orbiter fuselage without wings was tested at a freestream Mach number of 7.4 and angles of attack from 40° to 70°. The phase-change-paint technique was used to obtain heating data on the windward surface. The results are compared with theories for predicting heat transfer from laminar and turbulent boundary layers and the location of boundary layer transition. In addition, some effects of surface roughness on heating and transition have been simulated.

MODEL

Heat-transfer data were obtained on the windward surface of a 0.01-scale model of the Manned Spacecraft Center (MSC) orbiter body (fig. 1). The fuselage length was 43.82 cm., (17.25-in). The overall length, used to normalize axial distances and to determine model scale, was 46.69 cm., (18.38-in). The inclination and half-width of the bottom surface are shown in figure 2. The chine radius was 1.016 mm (0.040-in).

The model was cast with an aluminum-filled epoxy for which $\sqrt{\rho ck}$ = 441.5 joules/meter^2-(sec)$^{1/2}$-$^{\circ}$K (0.7 Btu/ft^2-(sec)$^{1/2}$-$^{\circ}$F). This value was determined by a comparison of temperature-sensitive-paint heating data and the thermocouple data of reference 1.

TEST PROCEDURE AND CONDITIONS

The temperature-sensitive-paint technique for determining heat transfer is described in reference 2. Briefly, it consists of determining the history and position of an isotherm (photographing a melt line), and with a knowledge of the thermophysical properties ($\sqrt{\rho ck}$) of the model material, deducing the heat transfer.

Tests were conducted in the Ames 3.5-foot hypersonic wind tunnel at a freestream Mach number of 7.4. A list of test conditions is given in Table I. Nominal total conditions were; temperature 722°K (1300°R) and pressure, 13.6 to 81.6 atmospheres. The angles of attack were 40°, 50°, 60°, and 70° measured between the wind vector and the surface of zero-degree inclination (fig. 2).

A number of tests was made in which small ($\frac{h}{\delta} < 1$) wires were placed across the windward surface of the model to simulate the effects of two-dimensional protuberances on heating and transition. The wires were 0.079-mm (0.0031-in) in diameter and were spaced at approximately 2.54-cm (1-in) intervals along the axis. The wire grid was replaced after each run because some of the wires would break. As a result, the grids are not located exactly the same from run to run and for a given run a few wires may be missing.

RESULTS AND DISCUSSION

The basic data are presented in figures 3 to 10 as contours of $\dot{q}/\dot{q}_s$ where $\dot{q}_s$ is the calculated stagnation-point heating rate on a reference hemisphere with a radius of 0.305 cm (0.120-in) (Table I). Each figure is for a specific angle of attack and consists of data at various Reynolds numbers. Although data are presented for the entire windward surface, only centerline results will be analyzed in detail. Laminar-heating predictions were made using infinite swept-cylinder theory with the velocity gradient modified to account for the flat surface and chine radius (ref. 3). For turbulent flow, the flatplate theory of Spalding and Chi (ref. 4) was used with the distance from the origin of turbulent flow adjusted to account for streamline divergence. The Spaulding and Chi theory was chosen because it gave the best prediction of heating for the theories examined in reference 1. The origin of turbulent flow was assumed to be the beginning of transition, and the Reynolds analogy factor was assumed to be 1.0 (a value experimentally verified in reference 5 by data on flat plates in the same facility. For both laminar and turbulent flow the local boundary-layer-edge conditions were taken to be those calculated on a swept sylinder at the same local angle of attack.

Comparisons of theoretical and experimental heating rates are given in figure 11. The laminar predictions are good over the angle-of-attack range. At $\alpha = 40^\circ$ the flow was entirely laminar at all Reynolds numbers. Boundary-layer transition occured at the higher angles and some turbulent flow occurred at $\alpha = 50^\circ$ and 60°. Turbulent estimates were made for $\alpha = 50^\circ$ and 60° at the high Reynolds number, however, the limited amount of data precludes any assessment of the Spalding and Chi theory.

Referring again to figures 3 to 10, it can be seen that off-centerline laminar heating increases as the chines are approached. As the Reynolds number is increased and the boundary layer becomes turbulent, the heating is fairly constant across the body, at a fixed axial location. This suggests that crossflow affects laminar more than turbulent heating; an observation that has been made both experimentally and theoretically in connection with simple shapes such as cones.

Some effects of roughness were simulated by placing small wires across the windward surface at approximately 2.54-cm (1-in) intervals

along the axis. The arrangement of the wires on the model surface does not simulate any proposed pattern of panel joints or corrigations. Rather, they illustrate the effects of discrete, two-dimensional roughnesses on the heating and boundary-layer transition. The wire influence was investigated at all angles of attack, and the data are shown in figure 12.

The data presented in fig. 12 illustrate that the effect of the wires on heating is a function of the state of the boundary layer (i.e., laminar, transitional, or turbulent). For example, in the transitional and turbulent portions of the boundary layer, there is considerable variation in heating rate between the wires. Whereas, for laminar flow the variation is no more than that on a smooth model. In the former instance, the magnitude of the variation in heating between wires appears to be proportional to the amount of turbulence in the boundary layer. Considering figure 12 (c) ($\alpha = 60^{\circ}$), there is almost no change in heating between wires at the start of transition, however, at the end of transition there is almost a 20% variation in the heating rate.

In an effort to gain some insight into the mechanism by which wires affect heating, nonsimilar boundary-layer solutions were generated using the program of reference 6. As described in reference 6 the program calculates a laminar boundary layer in two-dimensional flow, however, it was recently modified to permit the calculation of transitional and turbulent boundary layers. In addition an account was made for crossflow as described in reference 3. Ratios of wire height to boundary-layer thickness are indicated on the figure 8 for the different flow regimes. These results indicate that the wire heights are quite small relative to the boundary layer, particularly in turbulent flow. Although the relative height of the wires in the turbulent layer is less than the laminar layer their effect on turbulent flow is much greater, as indicated by the heating results. A similar observation can be made in figure 13.

Figure 13 is a shadowgraph of a section of the model at $\alpha = 50^{\circ}$ and at the high Reynolds number condition shown in figure 12 (b). As indicated in the figure, the boundary layer is initially laminar, undergoes transition, and is finally turbulent. Notice that in the laminar and initial portions of the transitional boundary layer the wires do not generate shock waves, however, in the turbulent portion they do. From the results of boundary-layer solutions, the undisturbed Mach number at the top of the wire at the beginning of transition was found to be 0.43; whereas, at the end of transition it was found to be 0.84. These results suggest that the increased effectiveness of the wires in the transitional and turbulent layers may be associated with the fuller velocity profiles of the turbulent boundary layer.

Other investigations on protuberances were examined to determine if similar observations could be made. However, the majority of the investigations were not applicable to the present situation. The theories of references 7 and 8 calculate the heating on the protuberance itself, whereas, in the present study the heating downstream of the disturbance

is of interest. Experimentally, the situation is much the same with the majority of the heating data being limited to the disturbance itself. In addition, the data are usually obtained on wavy walls where the height is of the order of the boundary-layer thickness or greater. In the present study the disturbance is much smaller than the boundary layer, as was shown earlier. Although the present data cannot be related to any previous work in the strictest sense, there are some interesting similarities. For example, in fig. 12 of reference 7 the heating downstream of a single, two-dimensional disturbance from which a turbulent boundary layer had separated and then reattached was found to be 30% greater than the undisturbed level at the reattachment point. This is very close to the maximum value measured immediately downstream of the wires in this investigation. In the same study and that of reference 8, it was found that sweeping the surface waves with respect to the flow, by as much as 70°, had no appreciable effect on the maximum value of heating on the wave itself. In the present study, the majority of the data show that at a fixed position downstream of a wire, turbulent heating is constant across the model even though the wires are effectively being swept with respect to the local flow (for local flow directions, see the streamline patterns of ref. 1).

Boundary Layer Transition

The majority of the data discussed previously contained examples of transition from laminar to turbulent flow. The location at which transition onset takes place is defined as the intersection of straight lines faired through the laminar and transitional portions of the heat transfer data. This location is used in conjunction with local-boundary-layer-edge properties to compare with proposed Space Shuttle transition criteria.

In figure 14 the transition data are compared with two transition criteria (refs. 9 and 10.) proposed during the earlier phases of the space shuttle preliminary design. These criteria evolved from wind-tunnel data on cones and delta wings and some flight data. The present, smooth-model data on an actual shuttle shape generally lie above these criteria; indicating a conservative prediction for the wind tunnel case. The rough-model transition data are included on this figure only for comparison with the smooth-model data and have no relationship to the criteria. However, a comparison of these data does indicate that at least this particular size and type of roughness is capable of significantly reducing the smooth-wall, transition Reynolds number.

CONCLUSIONS

Heat-transfer data on a 0.01-scale MSC orbiter body have been obtained at a freestream Mach number of 7.4 angles of attack of 40°, 50°, 60° and 70°, and for a Reynolds number range of 1.3 to 9 million. Some effects of surface roughness on heating and transition were simulated on the windward surface by placing 0.079 mm (0.0031-in) diameter wires

normal to the model axis. The data obtained on the windward centerline were analyzed and, the following is concluded:

1. Laminar heating rates are predicted quite well by modified swept-cylinder theory.
2. Initial boundary-layer transition correlations proposed for the space shuttle are somewhat conservative for the conditions of the present study.
3. The roughness used in this investigation was sufficient to cause premature transition.
4. Roughness heights less than the local boundary-layer thickness were sufficient to cause as much as a 20% increase in heating rate between wires in a transitional or turbulent boundary layer. No effect was observed when the flow was laminar.

REFERENCES

1. Marvin, J.G., Lockman, W.K., Mateer, G.G., Seegmiller, H.L., Pappas, C.C., DeRose, C.E., and Kaattari, G.E., "Flow Fields and Aerodynamic Heating of Space Shuttle Orbiters," NASA Space Shuttle Technology Conference, TMX 2272, vol. 1, pp. 21-71, April 1971.

2. Jones, R.A. and Hunt, J.L., "Use of Fusible Temperature Indicators for Obtaining Quantitative Aerodynamic Heat-Transfer Data," TR-R-230, 1966, NASA.

3. Marvin, J.G., Seegmiller, H.L., Lockman, W.K., Mateer, G.G., Pappas, C.C. and DeRose, C.E., "Surface Flow Patterns and Aerodynamic Heating on Space Shuttle Vehicles," AIAA Paper No. 71-594 presented at AIAA 4th Fluid and Plasma Dynamics Conference, June 21-23, 1971, Palo Alto, California.

4. Spalding, D.E., and Chi, S.W., "The Drag of a Compressible Turbulent Boundary Layer on a Smooth Flat Plate with and without Heat Transfer," J. Fluid Mech., Vol. 18, pt. 1, Jan. 1964, pp. 117-143.

5. Hopkins, E.J., Rubesin, M.W., Inouye, M., Keener, E.R., Mateer, G.G., and Polek, T.E., "Summary and Correlation of Skin-Friction and Heat-Transfer Data for a Hypersonic Turbulent Boundary Layer on Simple Shapes," NASA TN D-5089, June 1969.

6. Marvin, J.G., and Sheaffer, Yvonne S., "A Method for Solving the Non-similar Laminar Boundary-Layer Equations Including Foreign Gas Injection," NASA TN D-5516, 1969.

7. Bertram, M.H., Weinstein, L.M., Cary, A.M., Jr., and Arrington, J.R., "Heat Transfer to Wavy Wall in Hypersonic Flow," AIAA Journal, vol. 5, No. 10, Oct. 1967, pp. 1760-1767.

8. Jaeck, C.C., "Analysis of Pressure and Heat Transfer Tests on Surface Roughness Elements with Laminar and Turbulent Boundary Layers", also Savage, R.T., and Nagel, A.L., "Appendix A: Shallow Wave Theory for Laminar Flow," NASA CR-537, 1966.

9. Masek, R.V., "Boundary Layer Transition on Lifting Entry Vehicle Configurations at High Angle-of-Attack," NASA TMX-52876, Vol. 1, pp. 445-462, 1970.

10. Moote, J.D., "A Minimum Heating Flight Mode for High Lateral Range Space Shuttle Entries Including the Effects of Transition," NASA TMX-52876, Vol. 1, pp. 531-546, 1970.

Run No.	α, deg	p_t, $\frac{N}{m^2}$	p_t, psia	T_t, °K	T_t, °R	T_w, °K	T_w, °R	$(Re_L)_\infty$	$\dot{q}_s$, $\frac{W}{m^2}$	$\dot{q}_s$, $\frac{Btu}{ft^2/sec}$
80	40	1.455×10^6	211.1	831.1	1496	373.9	673	1.34×10^6	3.57×10^5	31.42
81		2.811	407.7	851.1	1532	373.9	673	2.48	5.17	45.51
82		5.617	814.7	831.1	1496	422.2	760	5.15	6.24	55.00
*85		1.441	209.0	711.1	1280	373.9	673	1.72	2.58	22.70
*89		3.530	512.0	771.1	1388	422.2	760	3.68	4.19	36.93
90	50	2.813	408.0	709.4	1277	422.2	760	3.36	3.02	26.91
91		5.670	822.4	720.0	1296	422.2	760	5.61	4.50	39.67
92		8.250	1197	750.0	1350	422.2	760	9.00	6.01	52.91
*93		2.806	407.0	741.7	1335	422.2	760	3.12	3.41	30.03
*94		1.448	210.0	688.9	1240	373.9	673	1.82	2.40	21.18
77	60	1.944	282.0	791.7	1425	422.2	760	1.94	3.30	29.10
78		4.190	607.7	860.0	1548	422.2	760	3.62	5.79	51.03
79		8.161	1184	851.1	1532	477.8	860	7.19	6.86	60.45
*104		2.130	309.0	781.1	1406	422.2	760	2.17	3.35	29.55
*105		2.792	405.0	711.1	1280	422.2	760	3.32	3.06	26.98
*106		3.509	509.0	688.9	1240	422.2	760	4.40	3.16	27.82
96	70	1.427	207.0	750.0	1350	373.9	673	1.56	2.88	25.33
98		2.813	408.0	720.0	1296	422.2	760	3.28	3.17	27.94
100		4.206	610.0	740.6	1333	422.2	760	4.68	4.16	36.63
*97		1.455	211.0	720.0	1296	373.9	673	1.70	2.66	23.44
*101		2.110	306.0	720.0	1296	422.2	760	2.46	2.75	24.20
*102		2.806	407.0	699.4	1259	422.2	760	3.43	2.94	25.91
*103		3.537	513.0	708.3	1275	422.2	760	4.24	3.41	30.06

*Wire trips

TABLE I

Test Conditions

$M_\infty = 7.4$

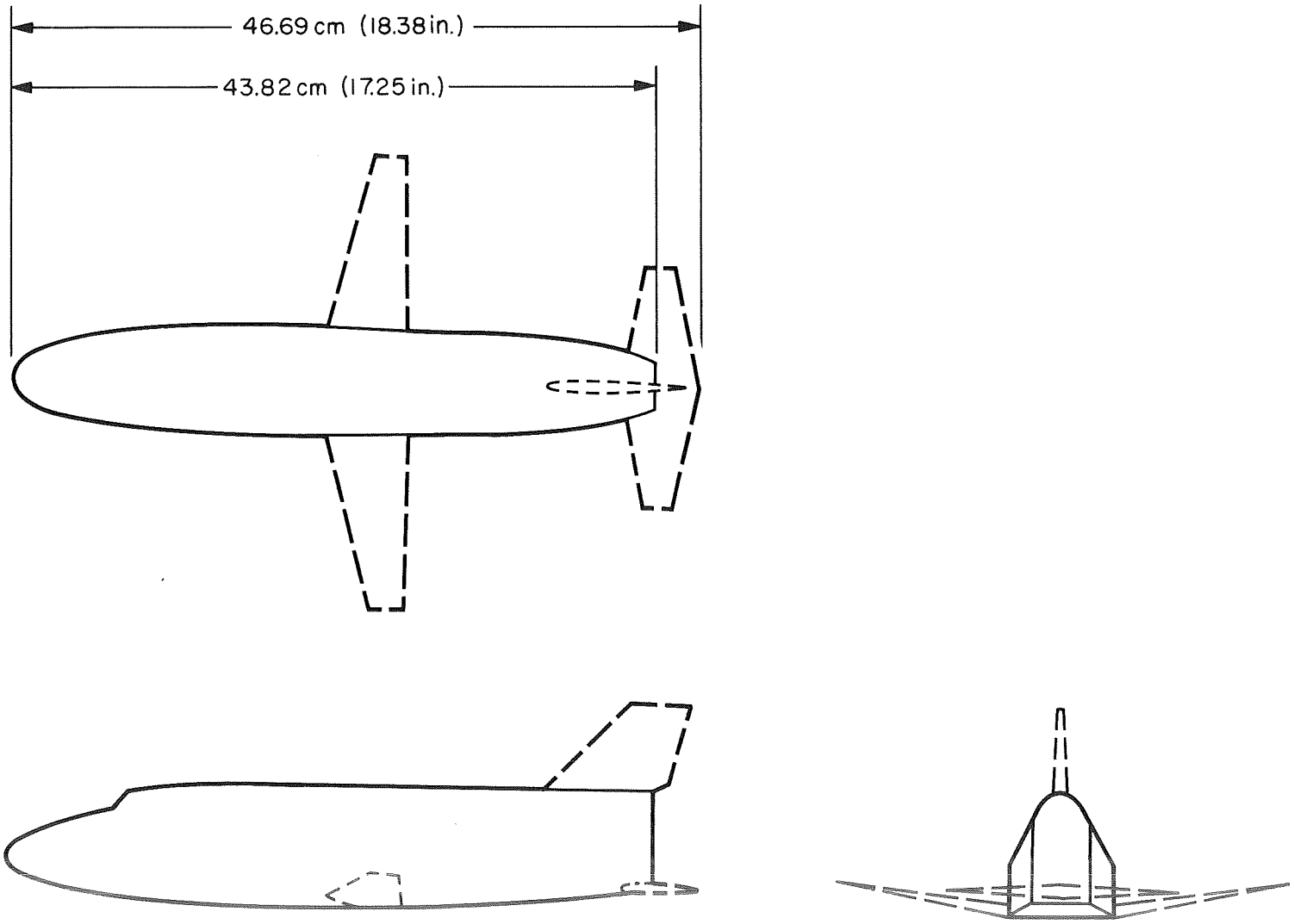

Figure 1. - MSC Shuttle Orbiter (test model body only).

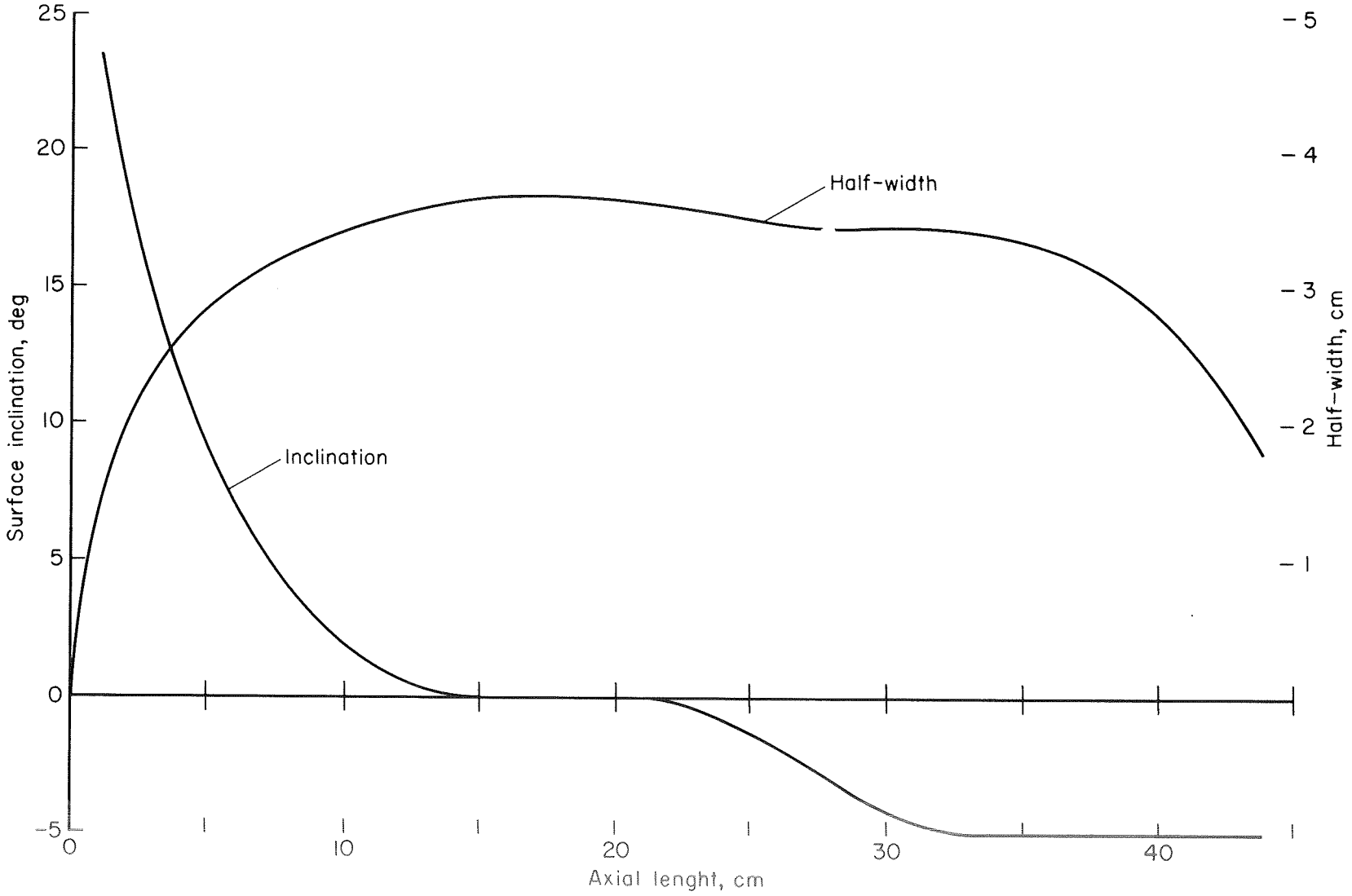

Figure 2. - Model geometry.

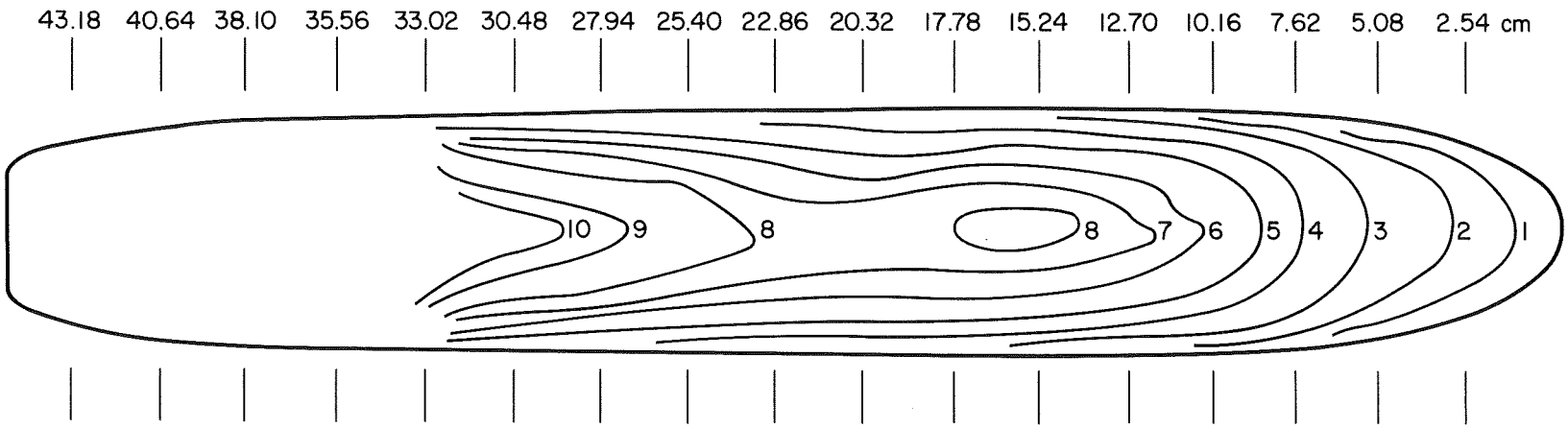

Run 80
$\alpha = 40°$

No.	$\dot{q}/\dot{q}_s$
1	0.1829
2	.1332
3	.1031
4	.0868
5	.0756
6	.0670
7	.0631
8	.0606
9	.0577
10	.0564

(a) $(Re_L)_\infty = 1.34 \times 10^6$

Figure 3. - Isotherms for smooth model; $\alpha = 40^o$.

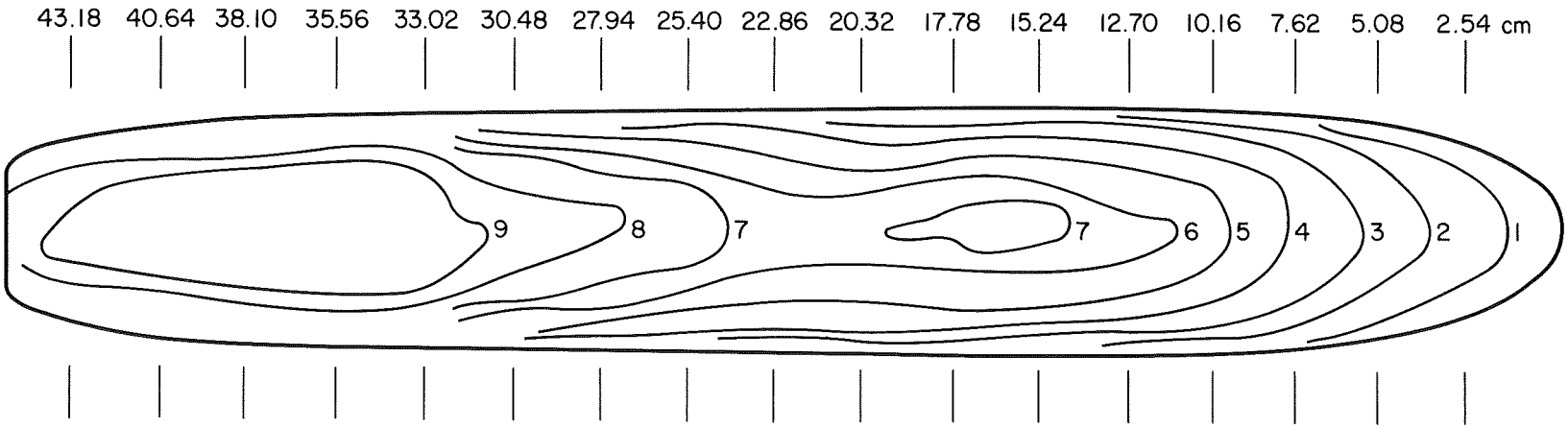

Run 81
$\alpha = 40°$

No.	$\dot{q}/\dot{q}_s$
1	0.1810
2	.1270
3	.1044
4	.0883
5	.0772
6	.0700
7	.0661
8	.0630
9	.0603

(b) $(Re_L)_\infty = 2.48 \times 10^6$

Figure 3. - Continued.

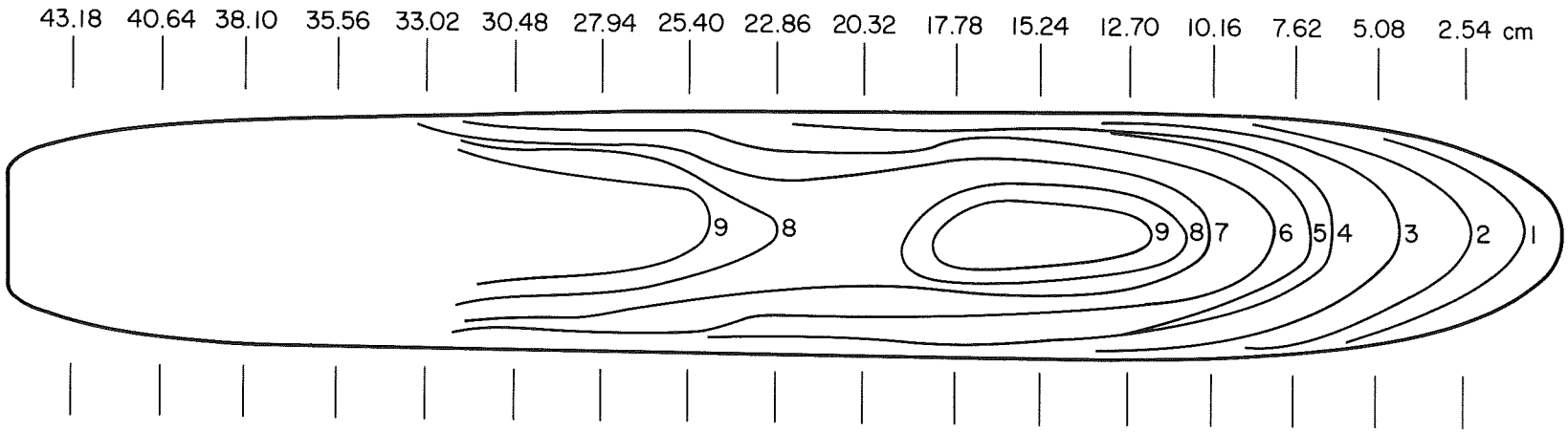

(c) $(Re_L)_\infty = 5.15 \times 10^6$

Figure 3. - Concluded.

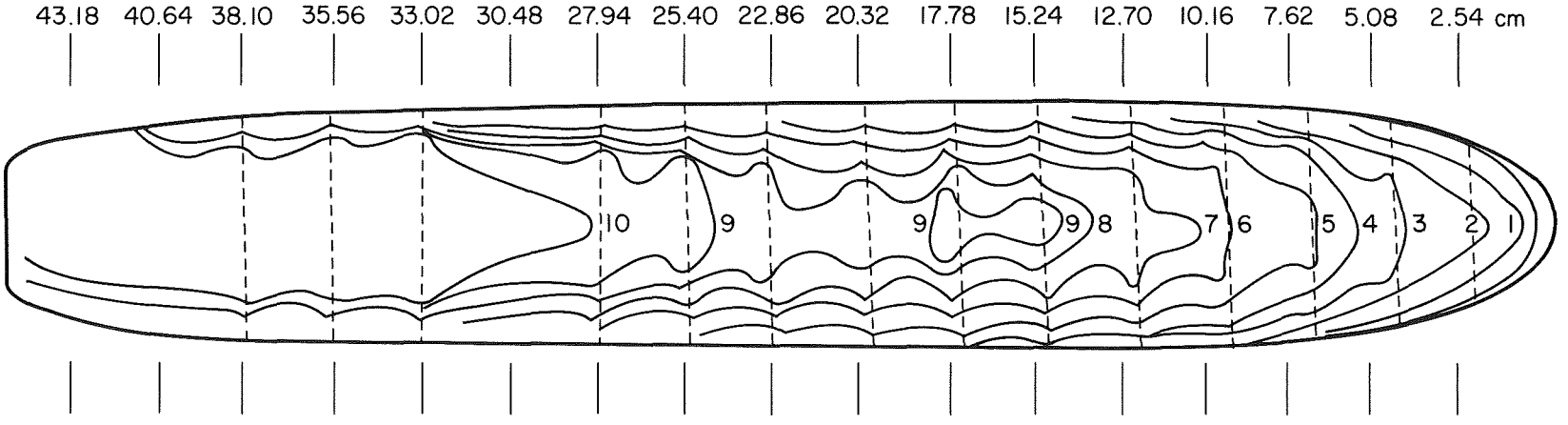

	No.	$\dot{q}/\dot{q}_s$
Run 85	1	0.2299
$\alpha = 40°$	2	.1595
	3	.1267
	4	.1075
	5	.0932
	6	.0795
	7	.0718
	8	.0679
	9	.0653
----- Wire locations	10	.0622

(a) $(Re_L)_\infty = 1.72 \times 10^6$

Figure 4. - Isotherms for rough model; $\alpha = 40^\circ$.

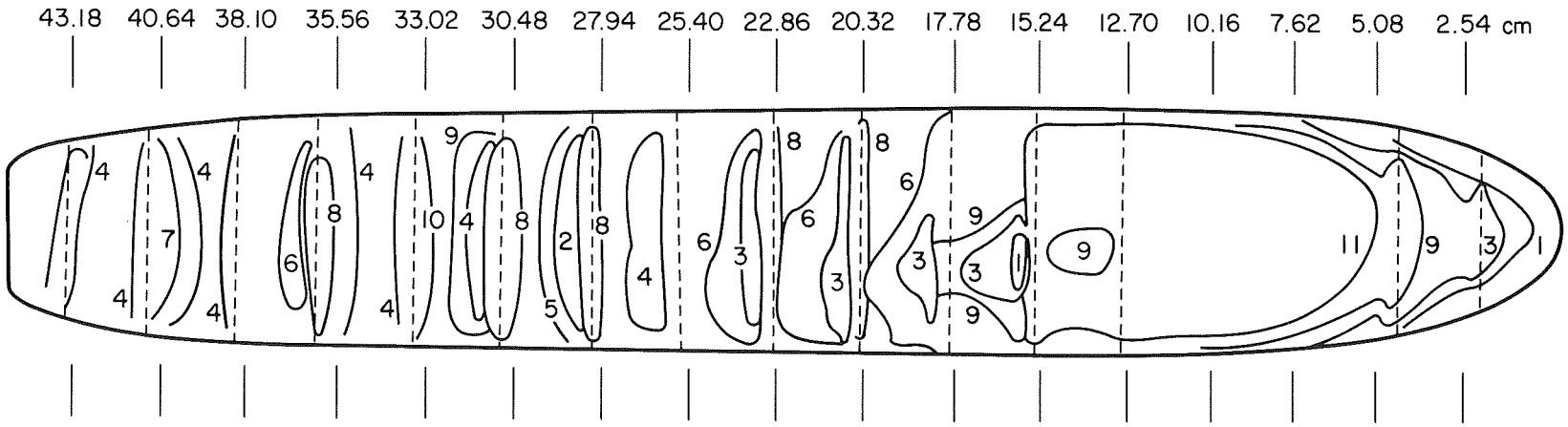

(b) $(Re_L)_\infty = 3.68 \times 10^6$

Figure 4. - Concluded.

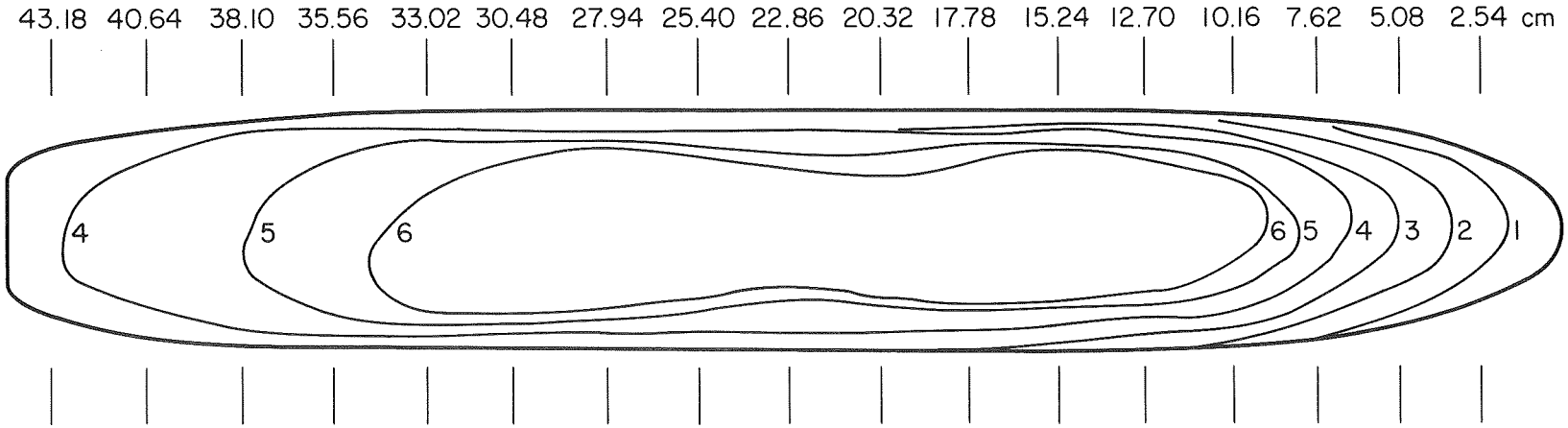

Run 90
$\alpha = 50°$

No.	$\dot{q}/\dot{q}_s$
1	0.1679
2	.1306
3	.1110
4	.0995
5	.0891
6	.0850

(a) $(Re_L)_\infty = 3.36 \times 10^6$

Figure 5. - Isotherms for smooth model; $\alpha = 50^\circ$.

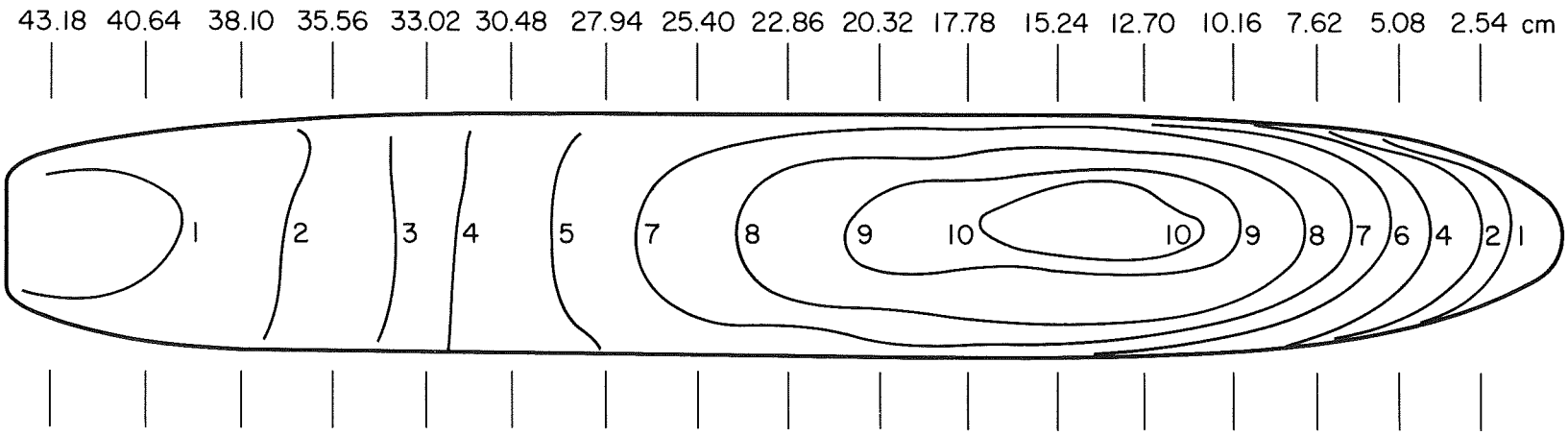

Run 91
$\alpha = 50°$

No.	$\dot{q}/\dot{q}_s$
1	0.2221
2	.1913
3	.1723
4	.1554
5	.1387
6	.1301
7	.1198
8	.1058
9	.0922
10	.0869

(b) $(Re_L)_\infty = 6.61 \times 10^6$

Figure 5. - Continued.

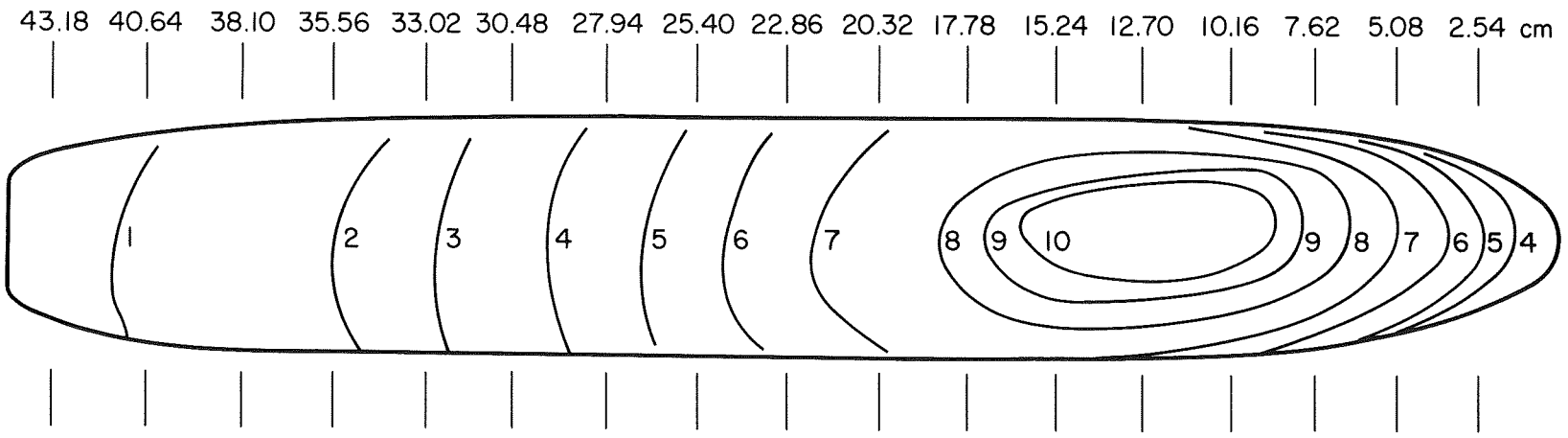

Run 92
$\alpha = 50°$

No.	$\dot{q}/\dot{q}_s$
1	0.2679
2	.2471
3	.2386
4	2239
5	.1922
6	.1602
7	.1355
8	.1148
9	.1053
10	.1008

(c) $(Re_L)_\infty = 9.0 \times 10^6$

Figure 5. - Concluded.

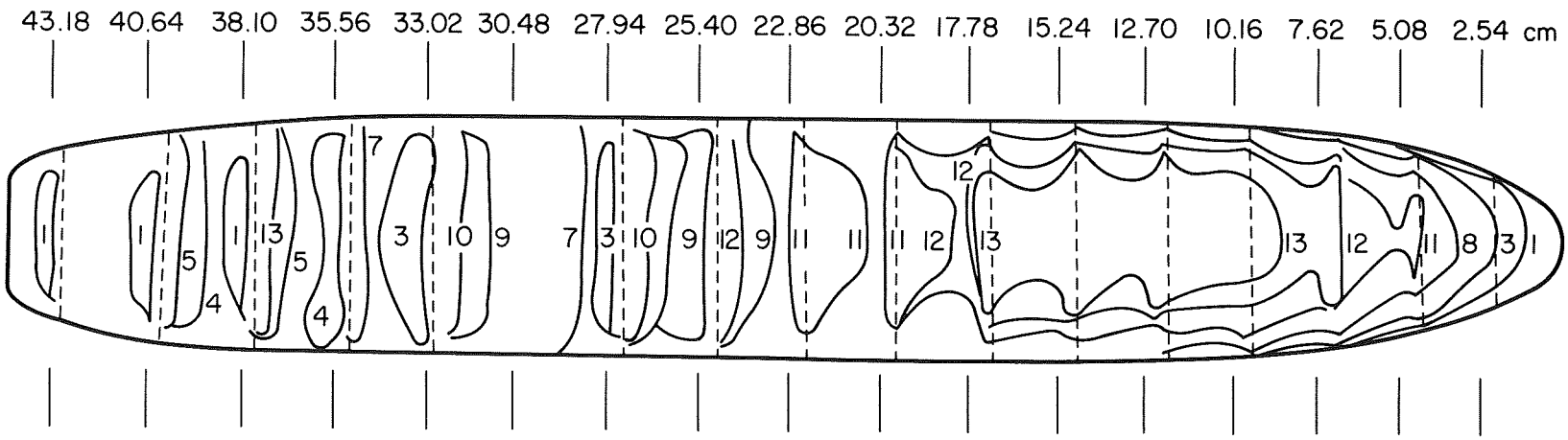

	No.	$\dot{q}/\dot{q}_s$
Run 93	1	0.2048
$\alpha = 50°$	2	.1810
	3	.1675
	4	.1657
	5	.1552
	6	.1516
	7	.1452
	8	.1406
	9	.1340
	10	.1270
	11	.1146
	12	.1004
---- Wire locations	13	.0879

(a) $(Re_L)_\infty = 3.12 \times 10^6$

Figure 6. - Isotherms for rough model; $\alpha = 50^\circ$.

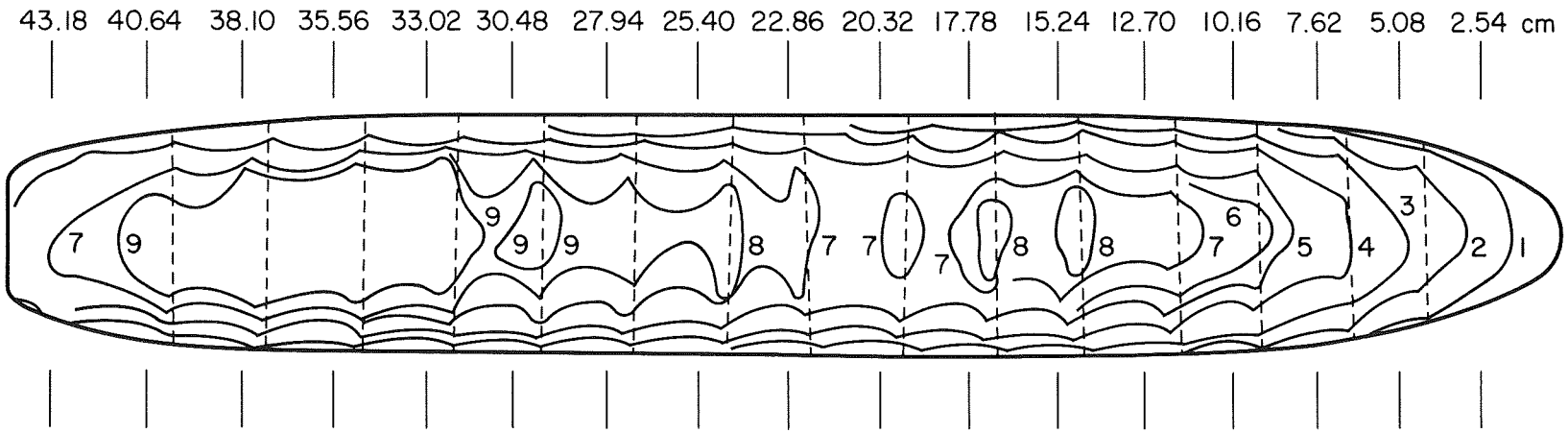

	No.	$\dot{q}/\dot{q}_s$
Run 94	1	0.2083
$\alpha = 50°$	2	.1651
	3	.1284
	4	.1111
	5	.0972
	6	.0907
	7	.0863
	8	.0820
----Wire locations	9	.0782

(b) $(Re_L)_\infty = 1.82 \times 10^6$

Figure 6. - Concluded.

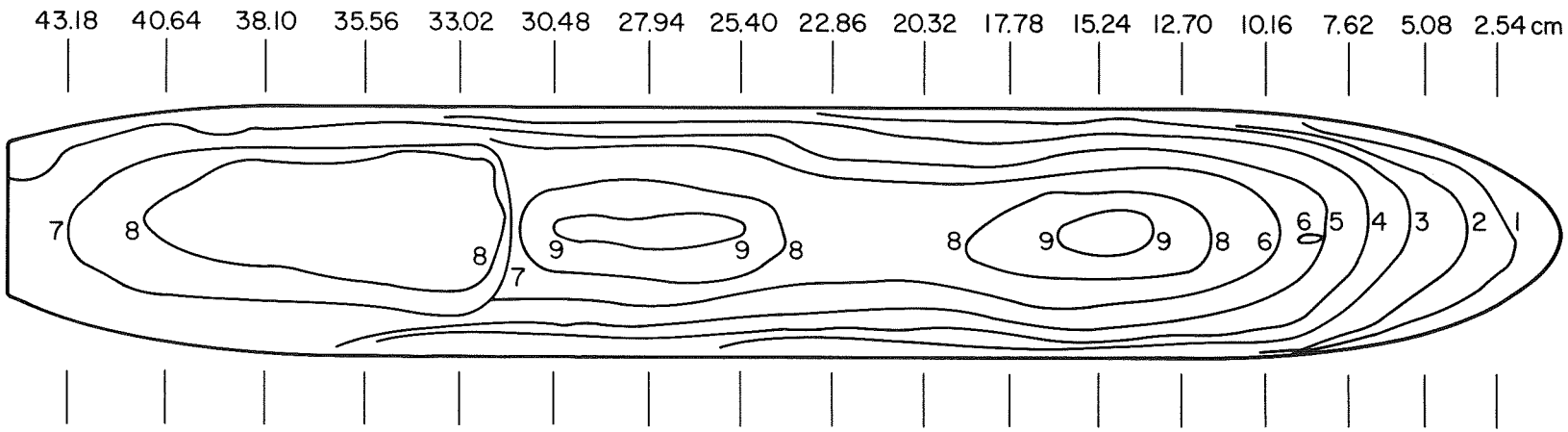

Run 77
$\alpha = 60°$

No.	$\dot{q}/\dot{q}_s$
1	0.1793
2	.1546
3	.1355
4	.1196
5	.1068
6	.0966
7	.0955
8	.0920
9	.0896

(a) $(Re_L)_\infty = 1.94 \times 10^6$

Figure 7. - Isotherms for smooth models, $\alpha = 60^\circ$.

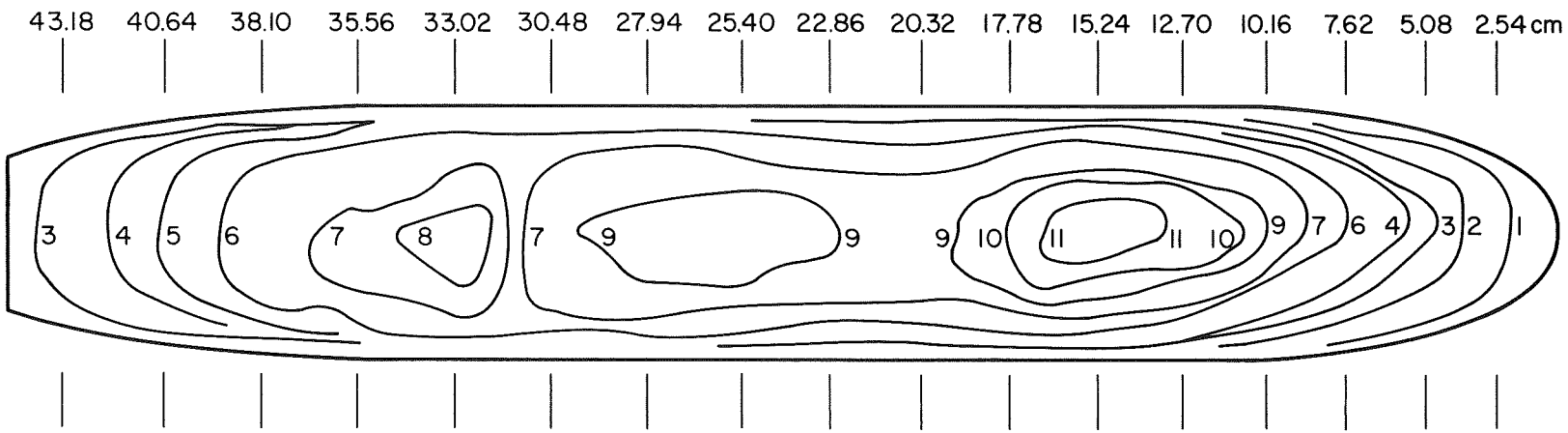

Run 78
$\alpha = 60°$

No.	$\dot{q}/\dot{q}_s$
1	0.2110
2	.1604
3	.1413
4	.1346
5	.1315
6	.1260
7	.1141
8	.1093
9	.1066
10	.1013
11	.0971

(b) $(Re_L)_\infty = 3.62 \times 10^6$

Figure 7. - Continued.

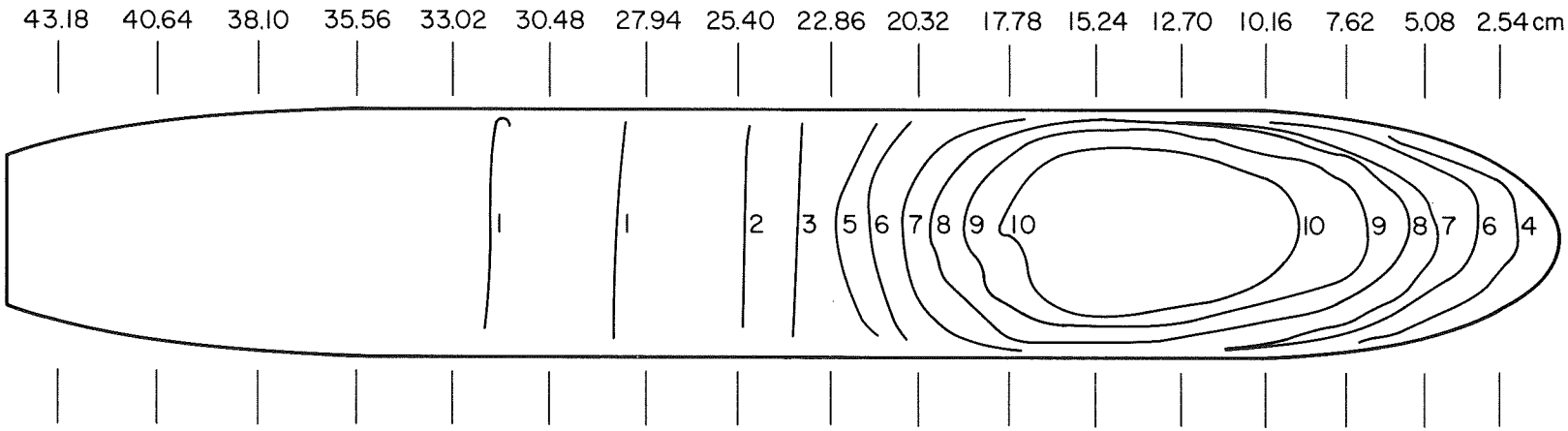

Run 79
$\alpha = 60°$

No.	$\dot{q}/\dot{q}_s$
1	0.2290
2	.2247
3	.1973
4	.1845
5	.1667
6	.1574
7	.1385
8	.1265
9	.1161
10	.1069

(c) $(Re_L)_\infty = 7.19 \times 10^6$

Figure 7. - Concluded.

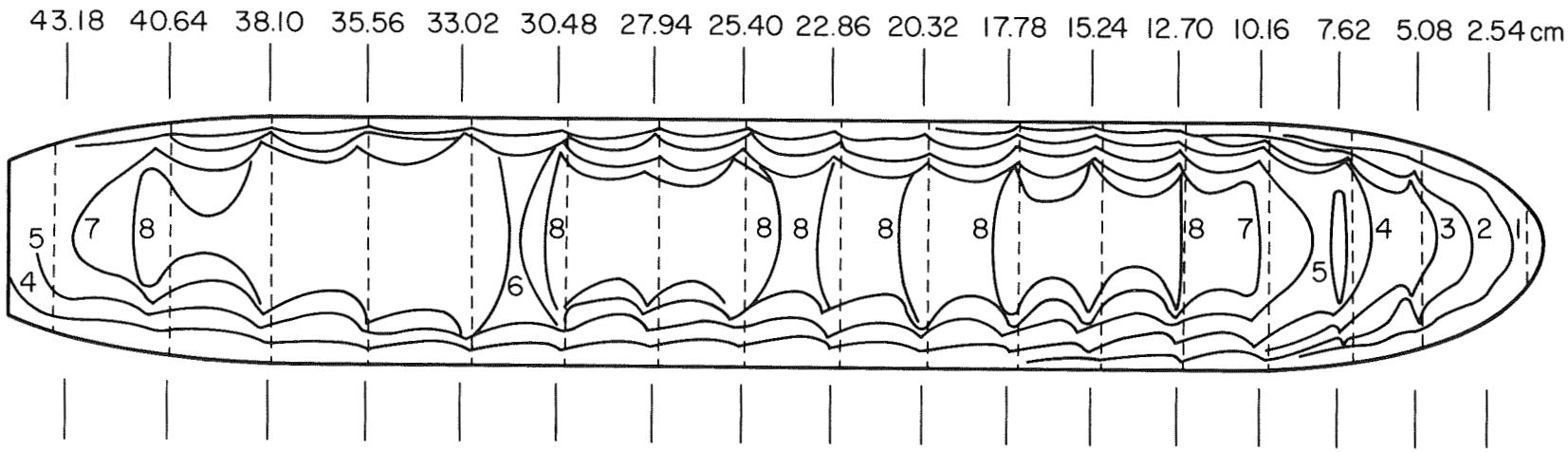

Run 104
$\alpha = 60°$

No.	$\dot{q}/\dot{q}_s$
1	0.1948
2	.1604
3	.1419
4	.1276
5	.1128
6	.1074
7	.1021
8	.0976

----Wire locations

(a) $(Re_L)_\infty = 2.17 \times 10^6$

Figure 8. - Isotherms for rough model; $\alpha = 60^\circ$.

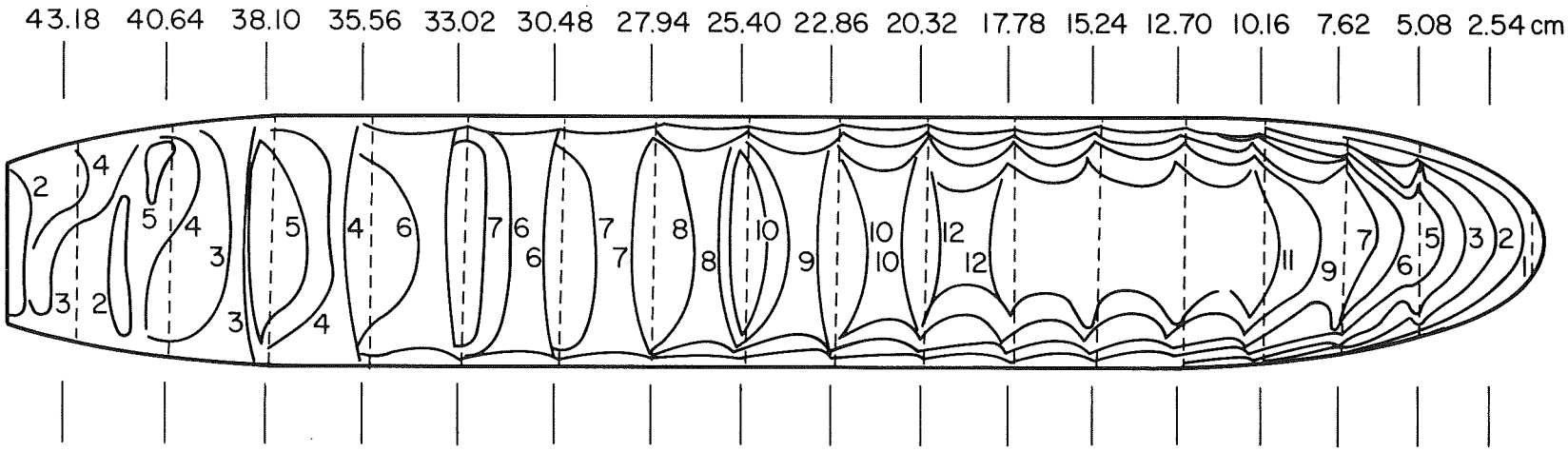

Run 105
$\alpha = 60°$

---- Wire locations

No.	$\dot{q}/\dot{q}_s$
1	0.1993
2	.1666
3	.1506
4	.1410
5	.1353
6	.1276
7	.1189
8	.1107
9	.1067
10	.1023
11	.0972
12	.0949

(b) $(Re_L)_\infty = 3.32 \times 10^6$

Figure 8. - Continued.

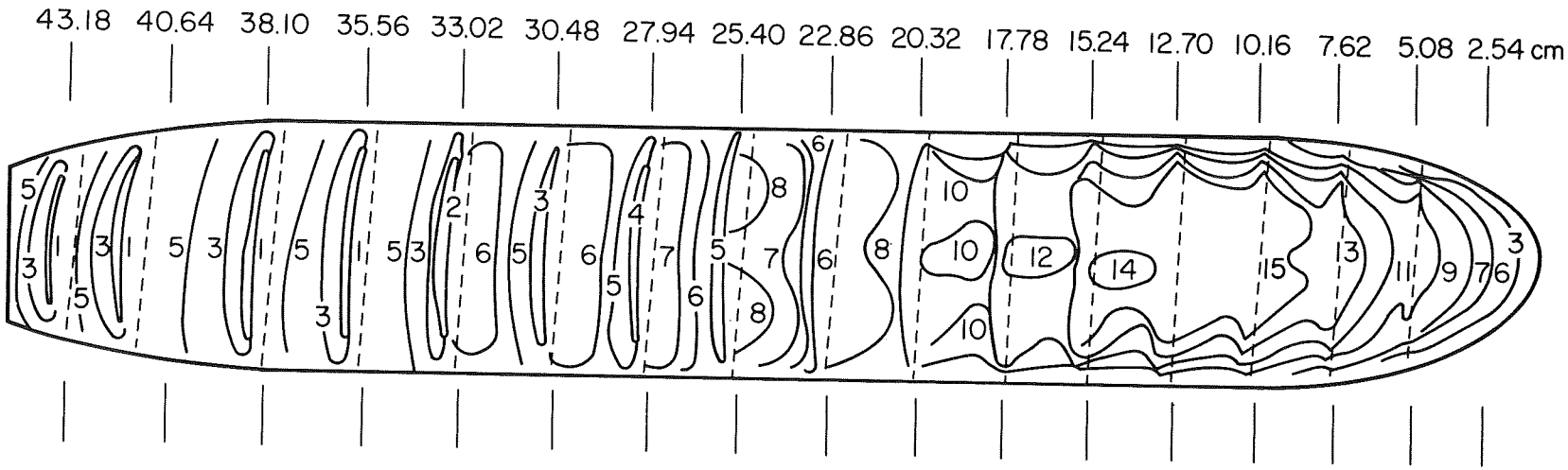

Run 106
$\alpha = 60°$

---- Wire locations

No.	$\dot{q}/\dot{q}_s$
1	0.2459
2	.2322
3	.2243
4	.2105
5	.2031
6	.1849
7	.1742
8	.1609
9	.1485
10	.1391
11	.1312
12	.1230
13	.1180
14	.1119
15	.1092

(c) $(Re_L)_\infty = 4.40 \times 10^6$

Figure 8. - Concluded.

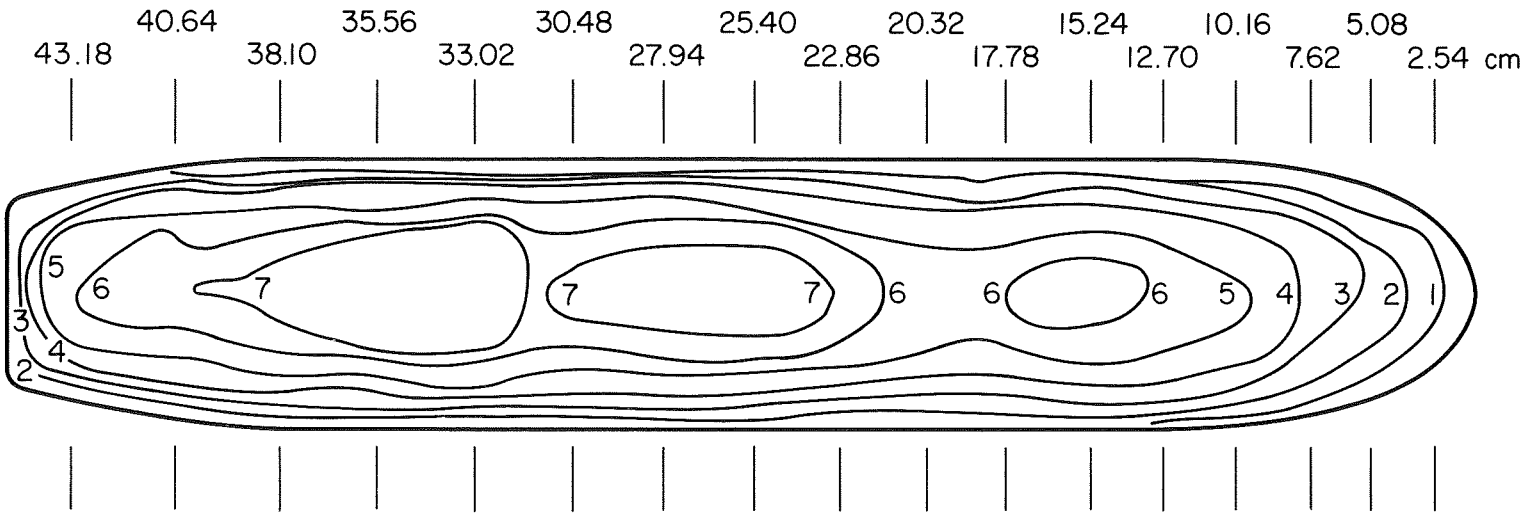

Run 96
α = 70°

No.	$\dot{q}/\dot{q}_s$
1	0.1858
2	.1578
3	.1419
4	.1306
5	.1192
6	.1139
7	.1092

(a) $(Re_L)_\infty = 1.56 \times 10^6$

Figure 9. - Isotherms for smooth models; $\alpha = 70^\circ$.

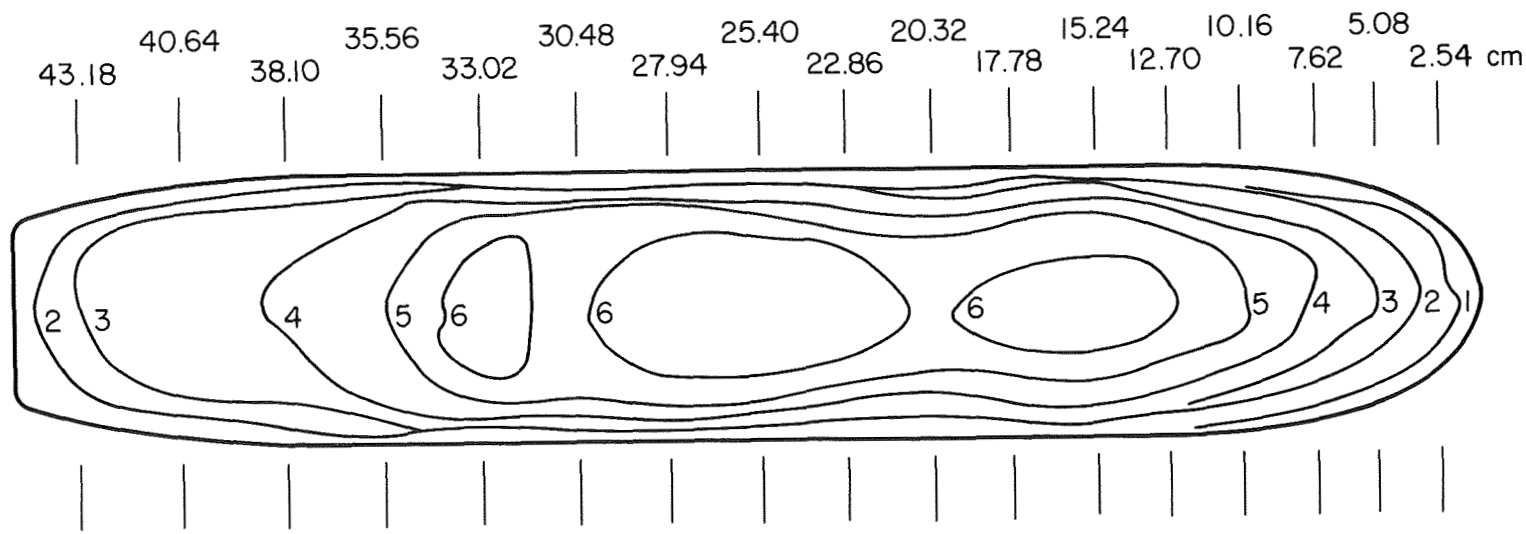

Run 98
α = 70°

No.	$\dot{q}/\dot{q}_s$
1	0.1770
2	.1478
3	.1379
4	.1269
5	.1194
6	.1089

(b) $(Re_L)_\infty = 3.28 \times 10^6$

Figure 9. - Continued.

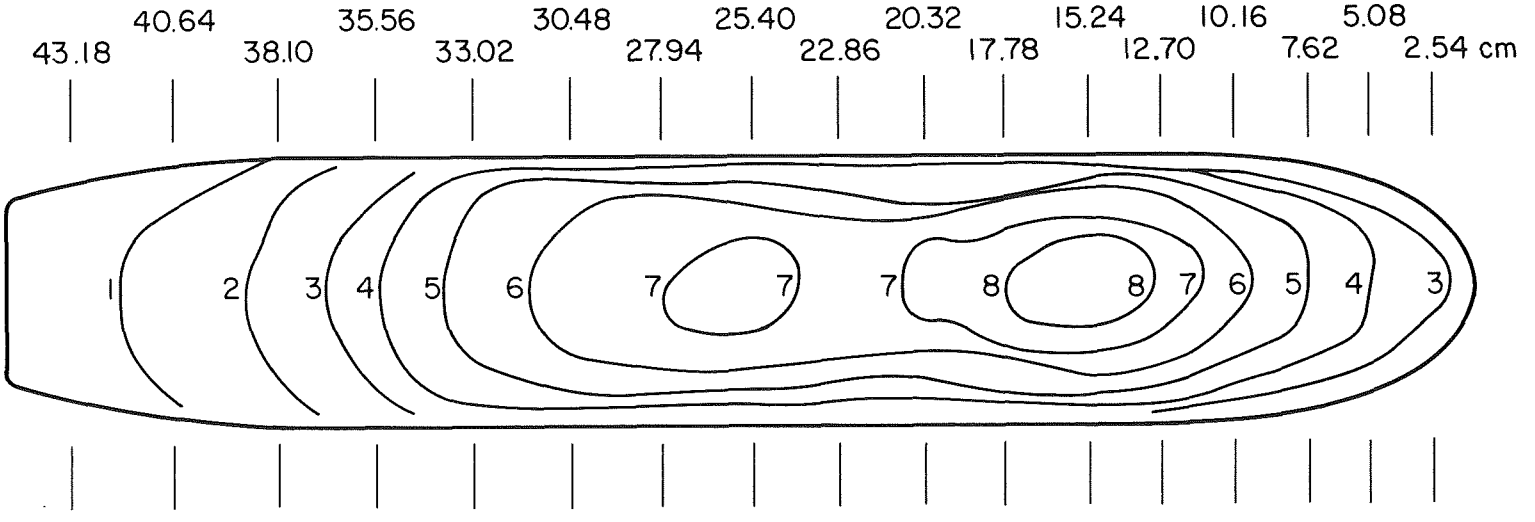

Run 100
$\alpha = 70°$

No.	$\dot{q}/\dot{q}_s$
1	0.2036
2	.1885
3	.1697
4	.1520
5	.1369
6	.1236
7	.1143
8	.1071

(c) $(Re_L)_\infty = 4.68 \times 10^6$

Figure 9. - Concluded.

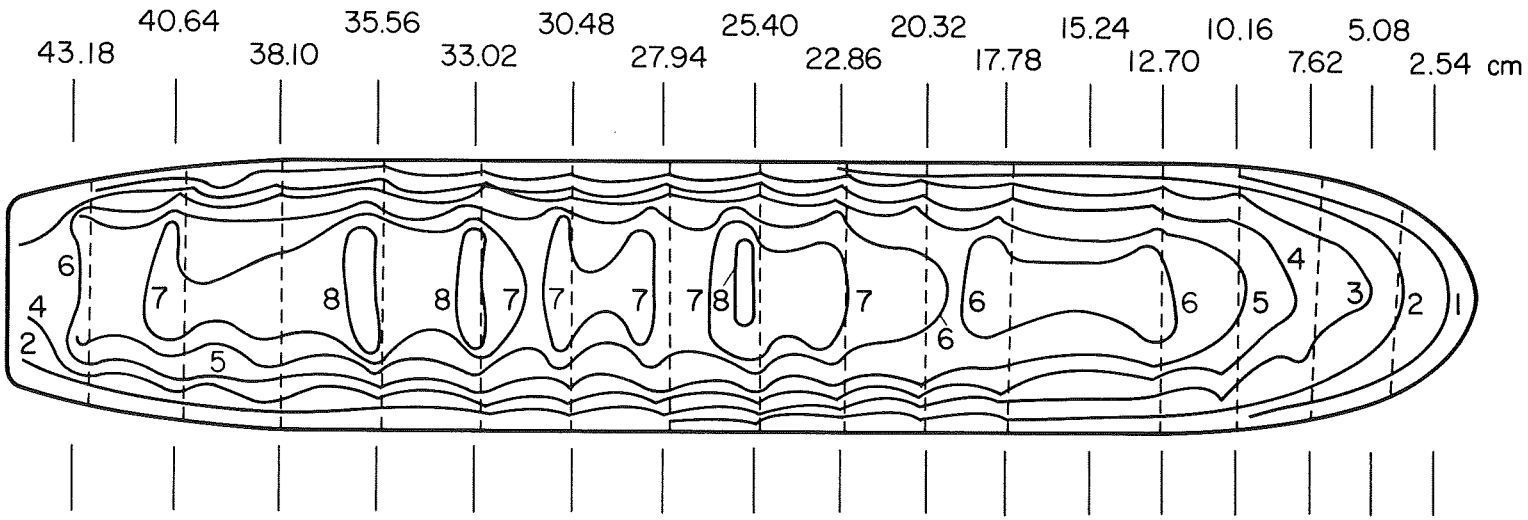

	No.	$\dot{q}/\dot{q}_s$
Run 97	1	0.1783
α = 70°	2	.1537
	3	.1340
	4	.1212
	5	.1119
	6	.1058
	7	.1012
---- Wire locations	8	.0947

(a) $(Re_L)_\infty = 1.70 \times 10^6$

Figure 10. - Isotherms for rough model; $\alpha = 70^\circ$.

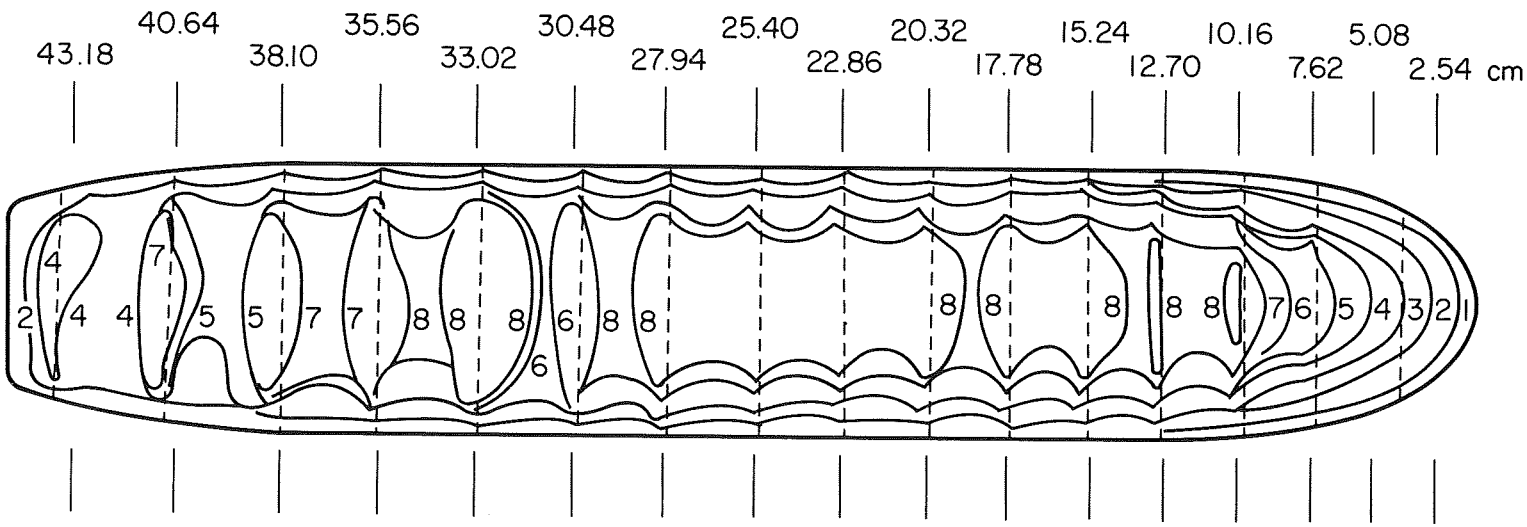

(b) $(Re_L)_\infty = 2.46 \times 10^6$

Figure 10 - Continued.

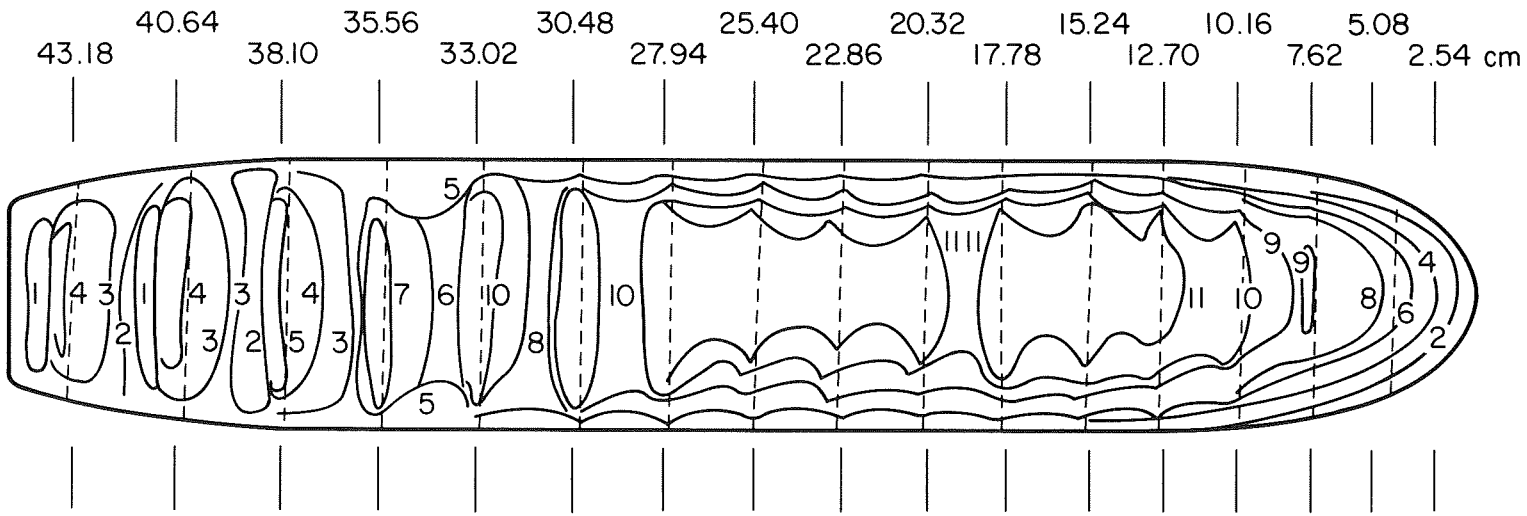

	No.	$\dot{q}/\dot{q}_s$
Run 102	1	0.2221
α = 70°	2	.1942
	3	.1828
	4	.1662
	5	.1595
	6	.1505
	7	.1463
	8	.1405
	9	.1273
	10	.1174
---- Wire locations	11	.1097

(c) $(Re_L)_\infty = 3.43 \times 10^6$

Figure 10. - Continued.

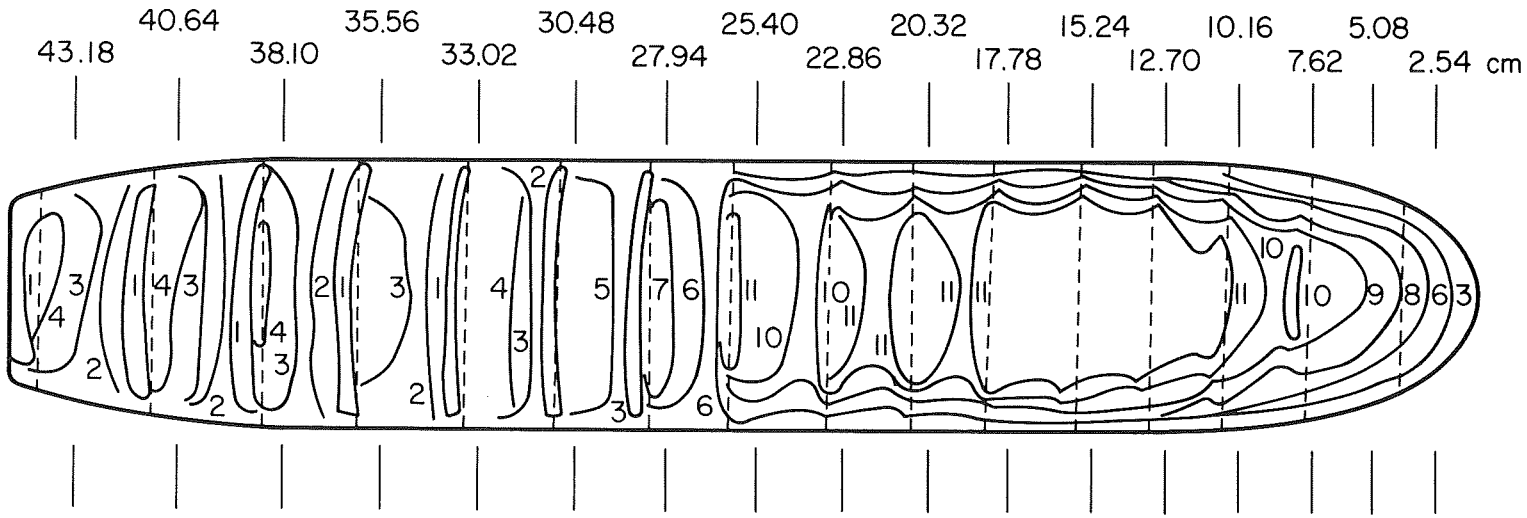

Run 103
$\alpha = 70°$

---- Wire locations

No.	$\dot{q}/\dot{q}_s$
1	0.2541
2	.2259
3	.2104
4	.2007
5	.1847
6	.1640
7	.1570
8	.1503
9	.1410
10	.1289
11	.1194

(d) $(Re_L)_\infty = 4.24 \times 10^6$

Figure 10. - Concluded.

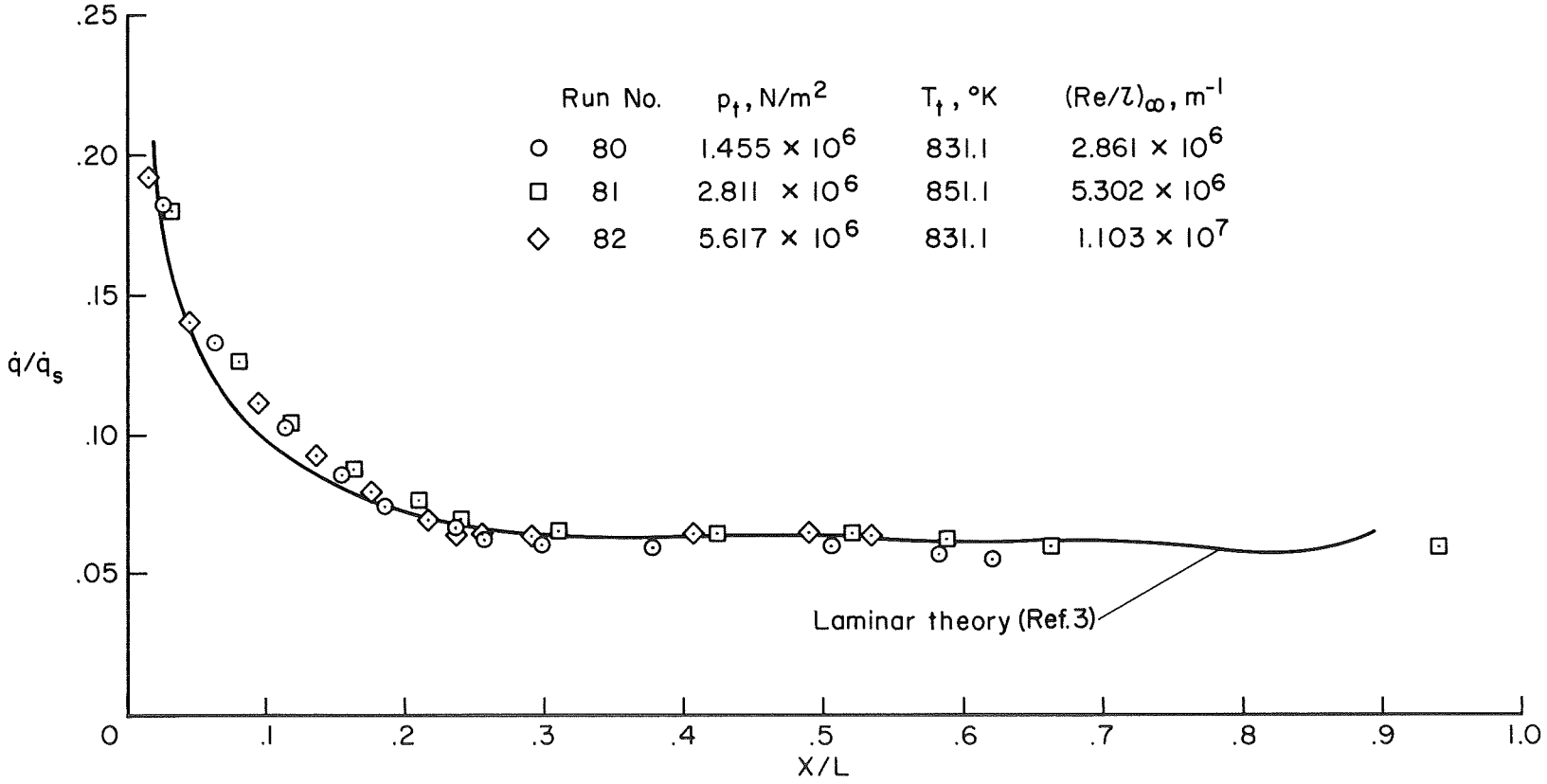

(a) $\alpha = 40^\circ$

Figure 11. - Heating distributions on MSC orbiter at $M_\infty = 7.4$.

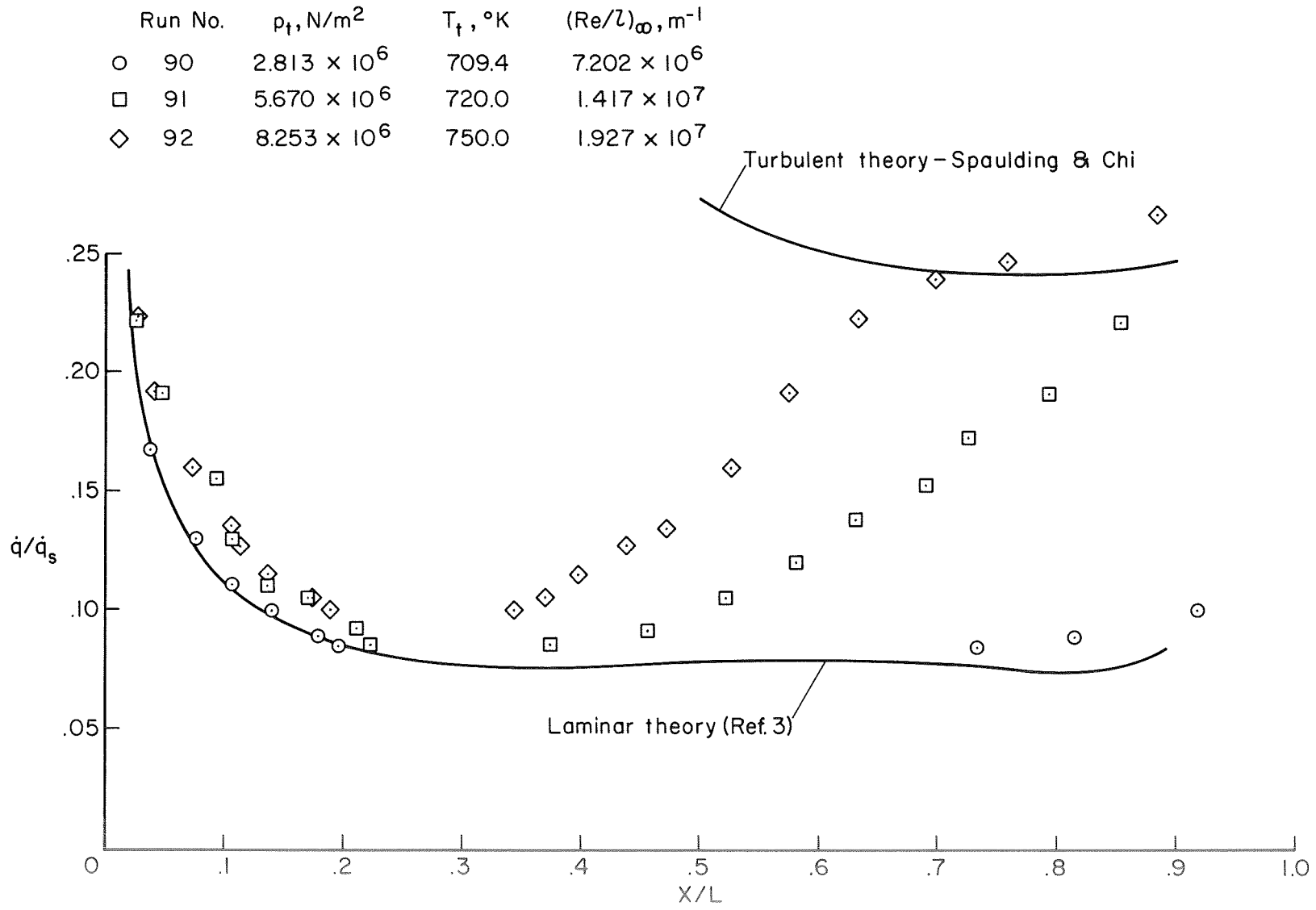

(b) $\alpha = 50^\circ$

Figure 11. - Continued.

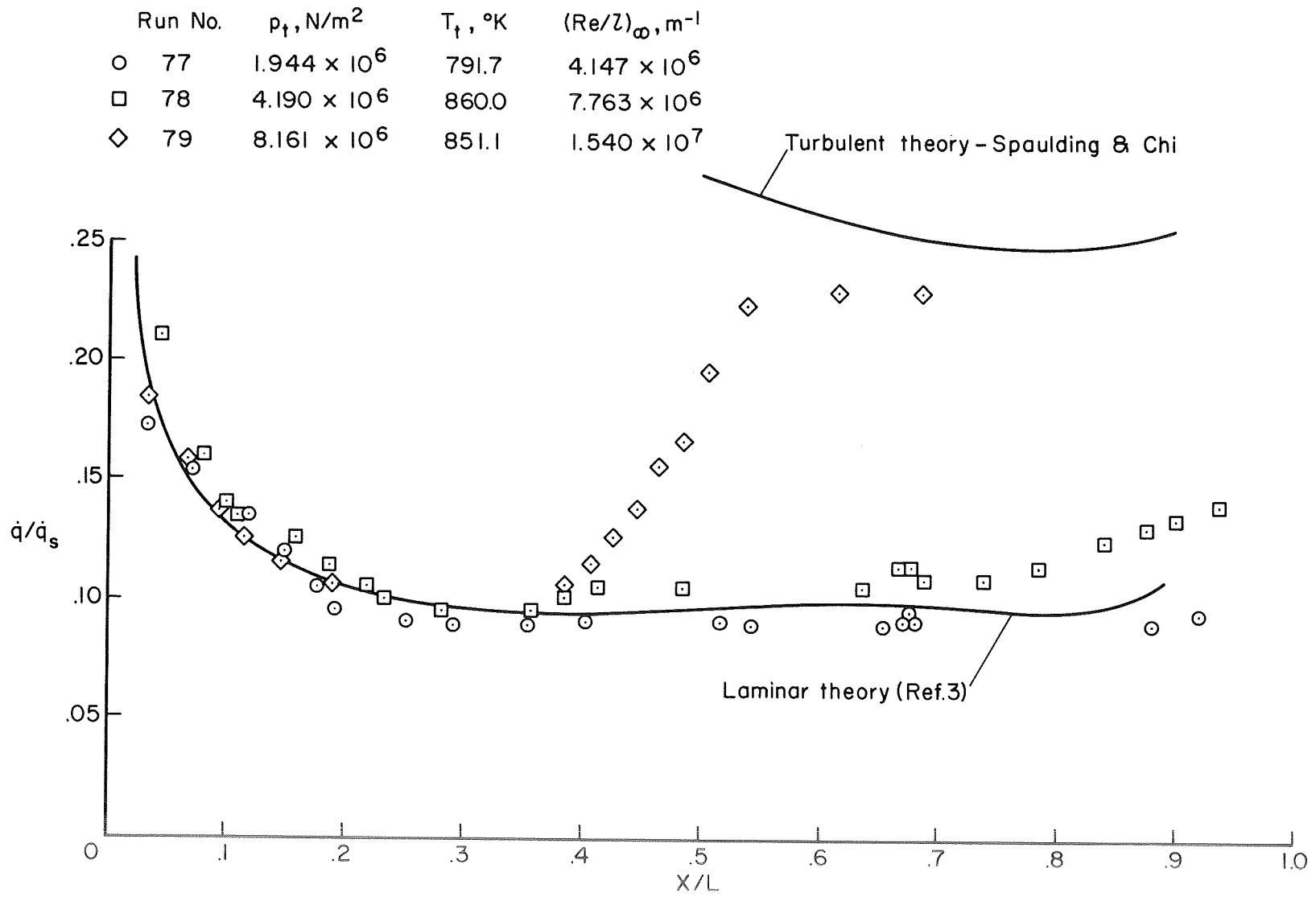

(c) $\alpha = 60^\circ$

Figure 11. - Continued.

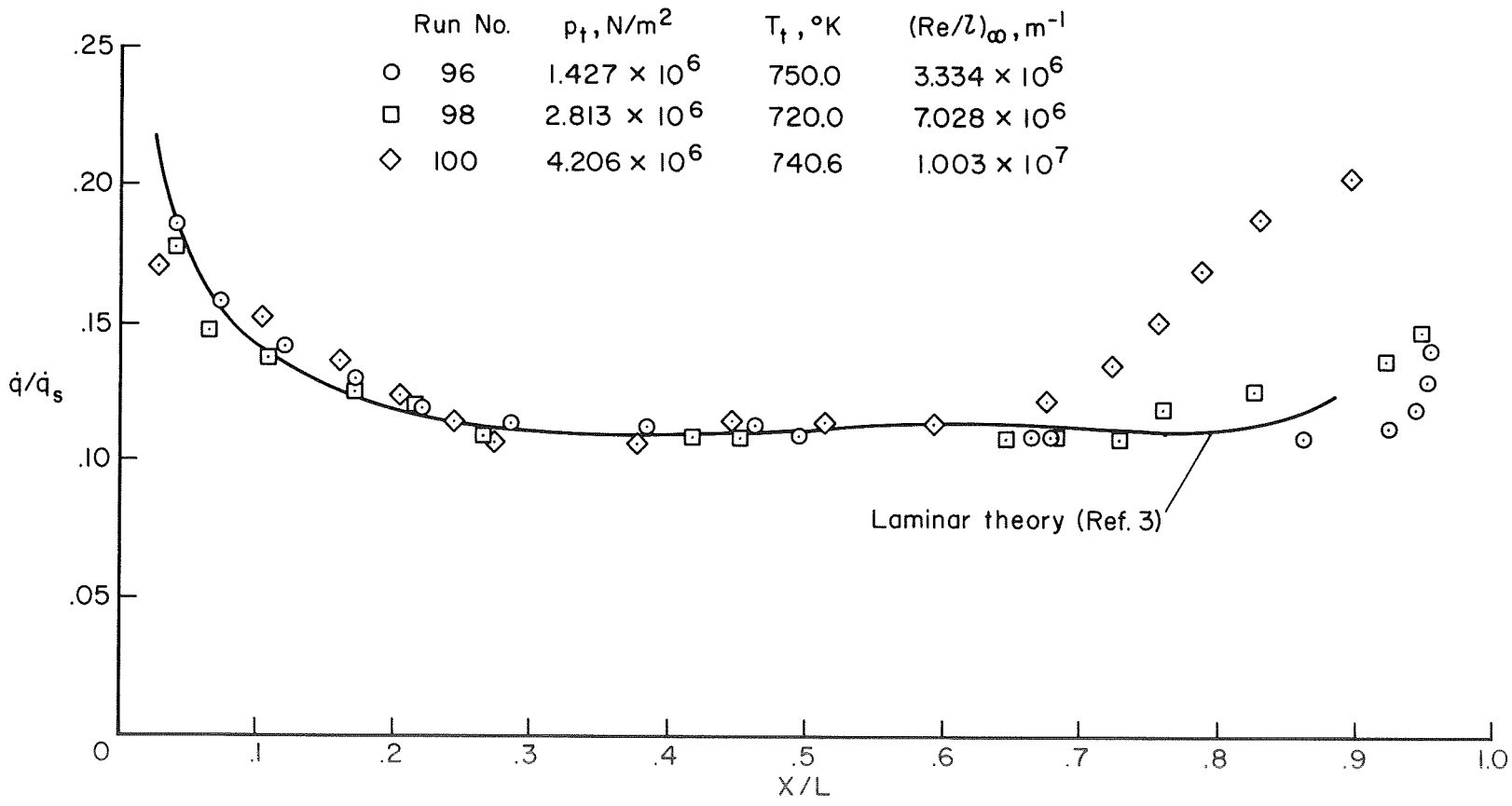

(d) $\alpha = 70^\circ$

Figure 11. - Concluded.

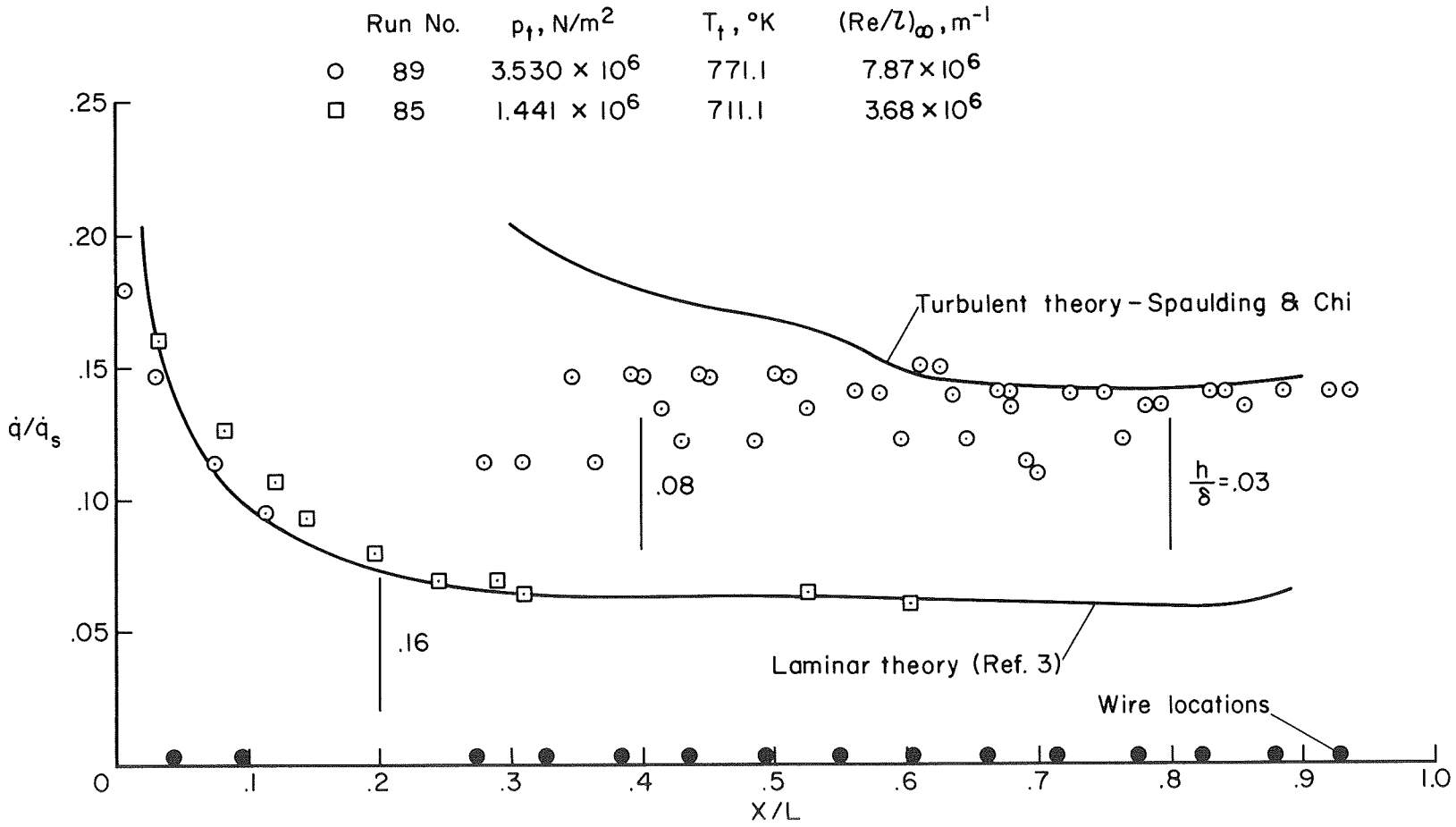

(a) $\alpha = 40^\circ$

Figure 12. - Effect of surface roughness on heating; MSC orbiter, $M_\infty = 7.4$.

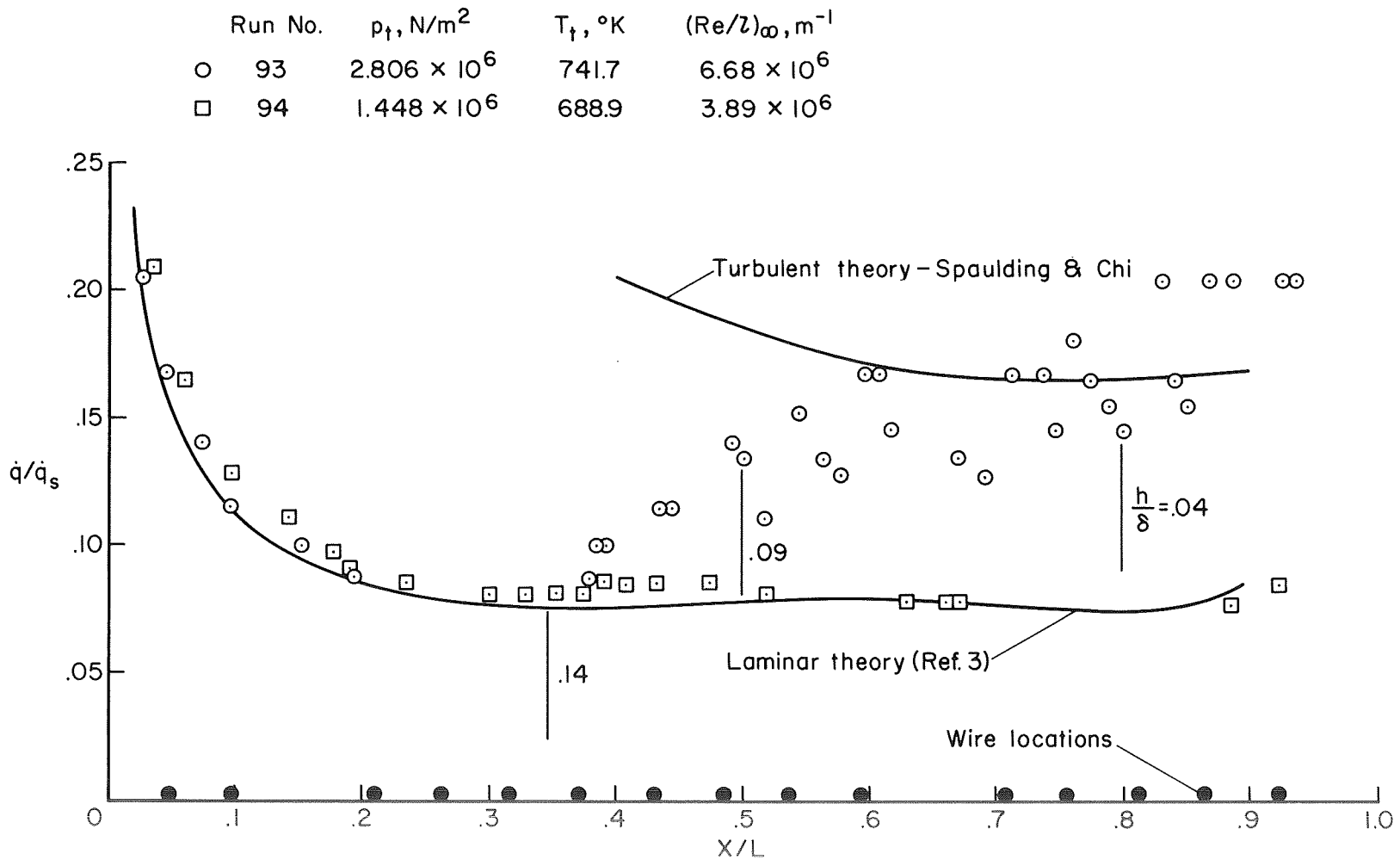

(b) $\alpha = 50^\circ$

Figure 12. - Continued.

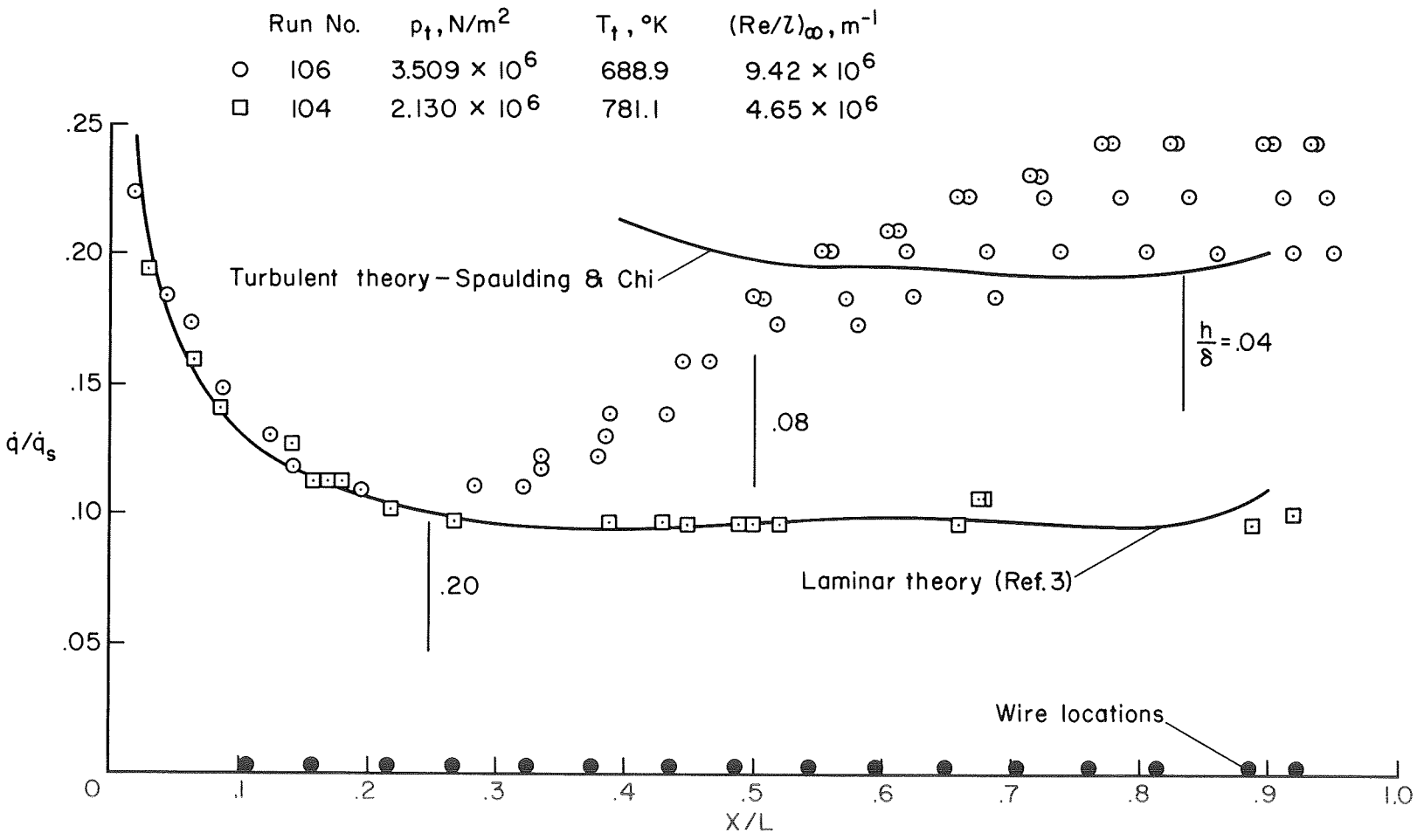

(c) $\alpha = 60^\circ$

Figure 12. - Continued.

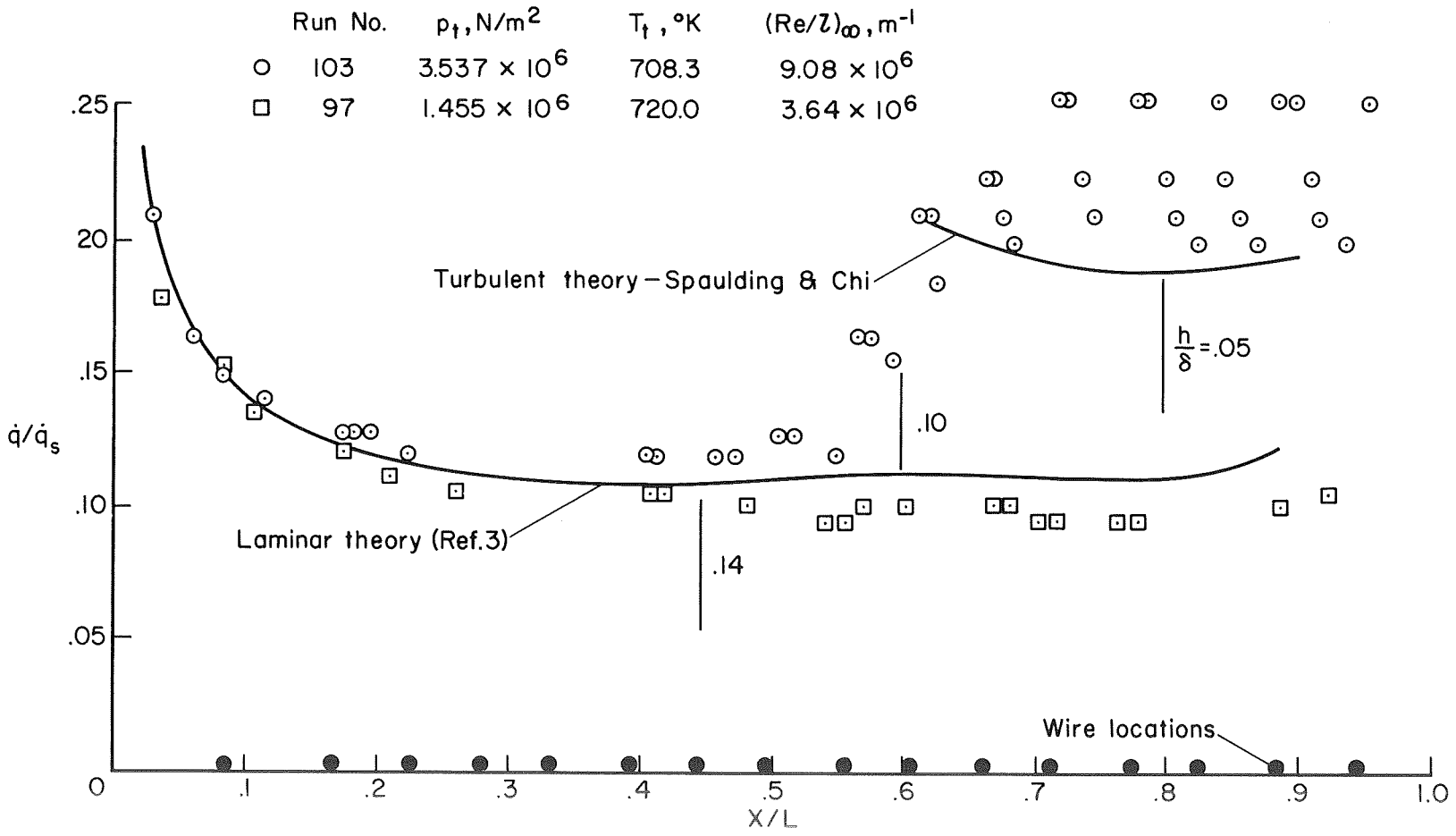

(d) $\alpha = 70^\circ$

Figure 12. - Concluded.

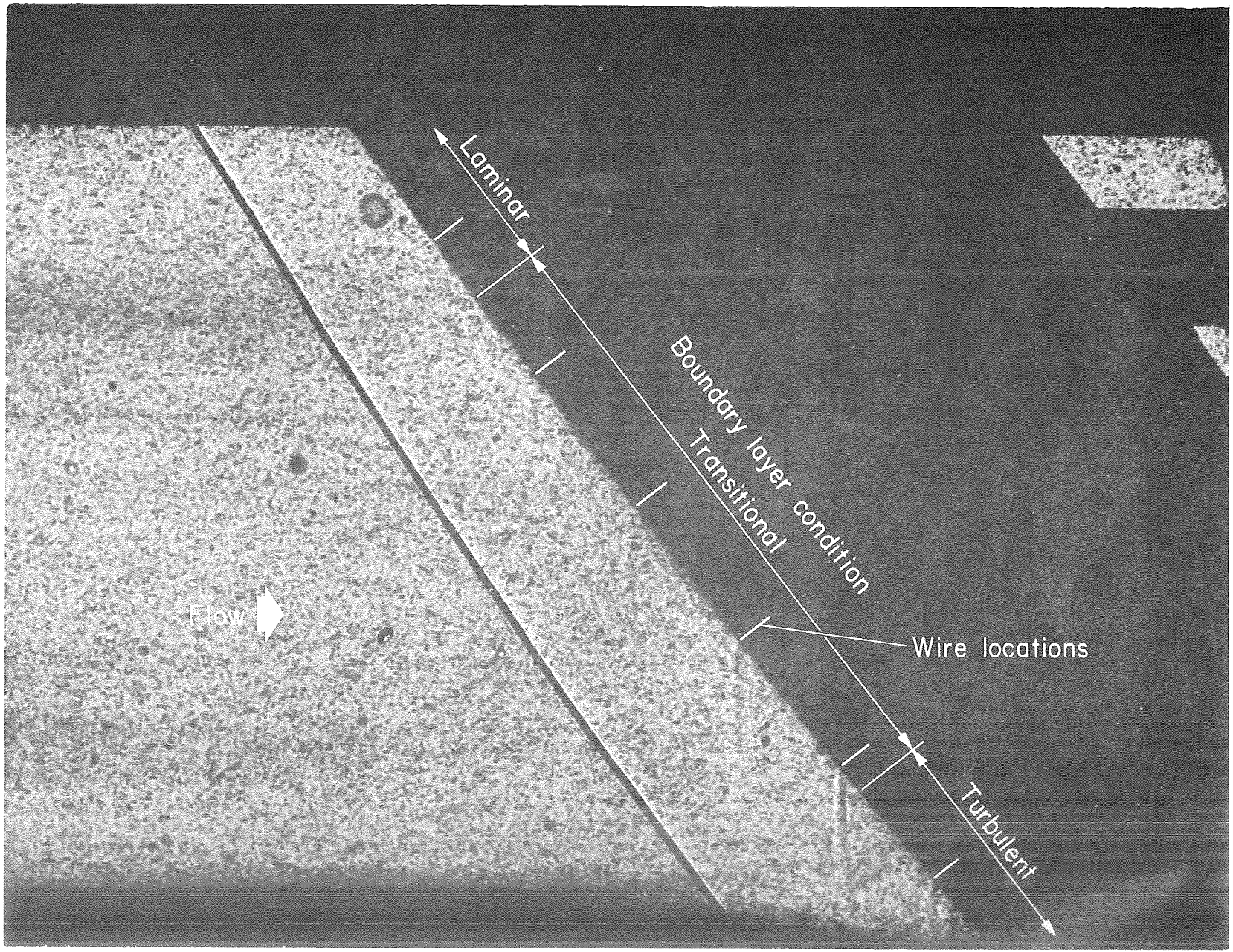

Figure 13. - Shadowgraph of MSC orbiter body, .32 < X/L < .62, M_∞ = 7.4, $\alpha = 50^\circ$, $(Re/\ell)_\infty = 6.7 \times 10^6$ m^{-1}.

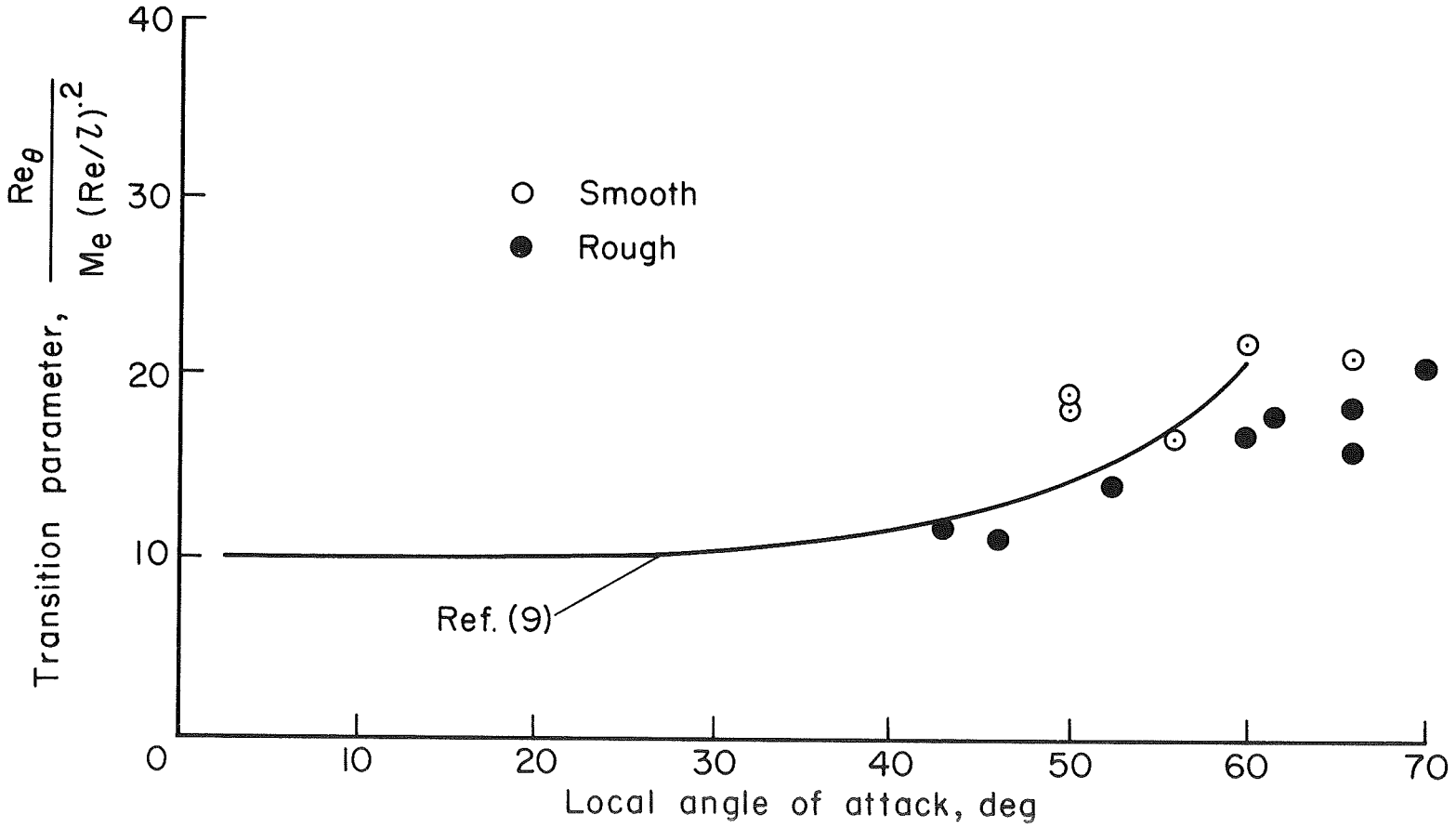

(a) Transition parameter vs. local angle of attack

Figure 14. - Comparison of transition data with proposed criteria.

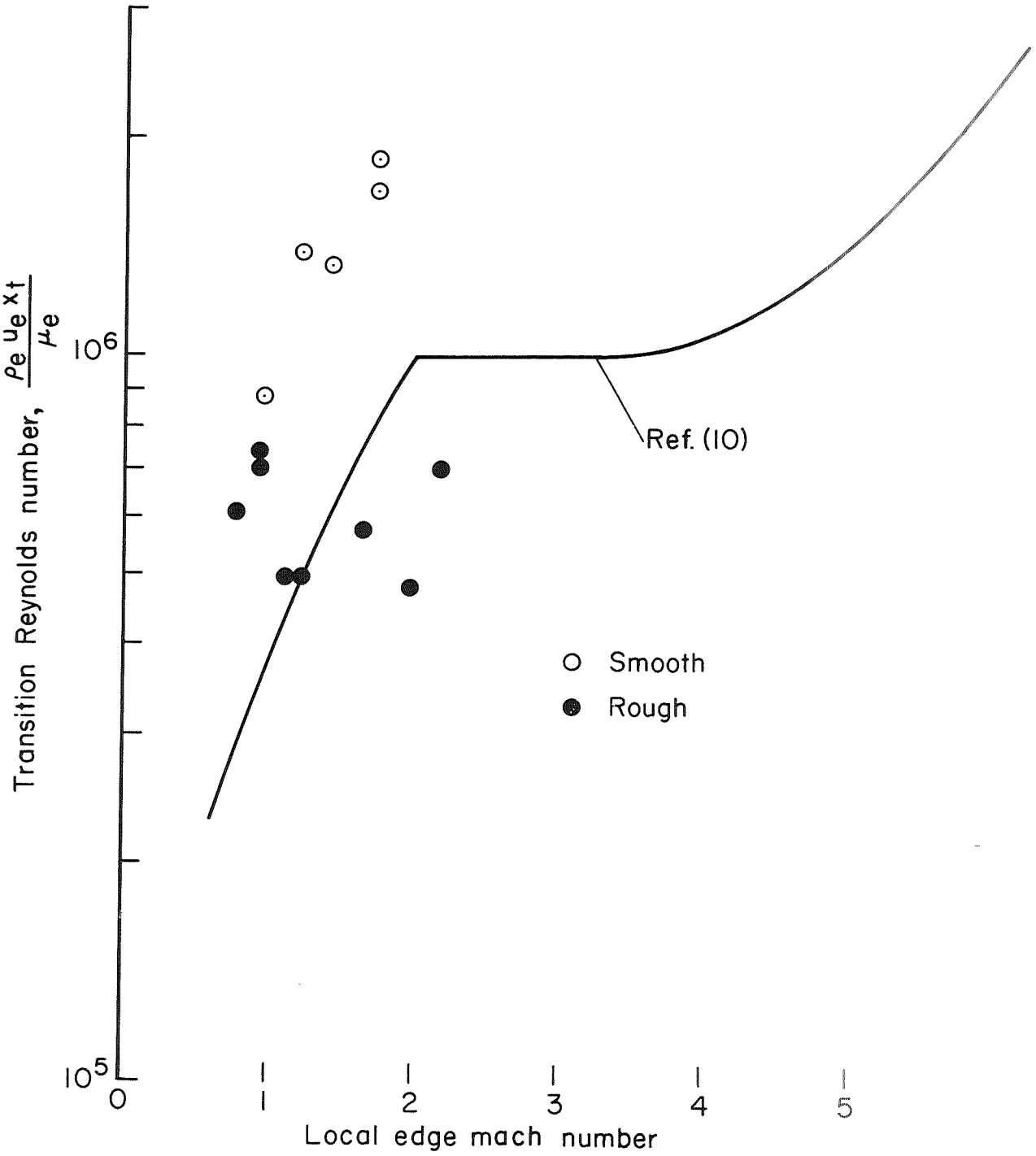

(b) Transition Reynolds number vs. local Mach number.

Figure 14. - Concluded.